To the Graduate Council:

I am submitting herewith a thesis written by Greg J. Ball entitled "An Adaptive Hysteresis Band Pulse Width Modulated Inverter Induction Motor Drive." I have examined the final copy of this thesis for form and content and recommend that it be accepted in partial fulfillment of the requirements for the degree of Master of Science, with a major in Electrical Engineering.

B. K. Bose, Major Professor

We have read this thesis
and recommend its acceptance:

Accepted for the Council:

Vice Provost
and Dean of The Graduate School

STATEMENT OF PERMISSION TO USE

In presenting this thesis in partial fulfillment of the requirements for a Master's degree at the University of Tennessee, Knoxville, I agree that the Library shall make it available to borrowers under rules of the Library. Brief quotations from this thesis are allowable without special permission, provided that accurate acknowledgment of the source is made.

Permission for extensive quotation from or reproduction of this thesis may be granted by my major professor, or in his absence, by the Head of Interlibrary Services when, in the opinion of either, the proposed use of the material is for scholarly purposes. Any copying or use of the material in this thesis for financial gain shall not be allowed without my written permission.

Signature Greg J Ball

Date July 25, 1990

AN ADAPTIVE HYSTERESIS BAND PULSE WIDTH MODULATED INVERTER INDUCTION MOTOR DRIVE

A Thesis

Presented for the

Master of Science

Degree

The University of Tennessee, Knoxville

Greg J. Ball

August 1990

ACKNOWLEDGMENTS

I am indebted to several people for their generous help during the course of this project. First, I would like to thank professors J. S. Lawler and J. M. Googe for serving on my supervisory committee and for providing me with the necessary encouragement and criticism. I am truly grateful to Dr. Jih-Sheng Lai, who, in patiently assisting me with technical problems, proved to be a consistent source of good advice. I would also like to thank Syd Ball, Ron Lambert and Lisa Wolfenbarger for their invaluable help in preparing the written thesis.

Most of all I wish to thank my advisor, B. K. Bose, for introducing me to this topic and introducing the university to power electronics. His consultation and support throughout made the completion of this project possible.

ABSTRACT

An adaptive hysteresis band pulse width modulated inverter drive for an induction motor is designed and developed in this thesis. Existing constant hysteresis band controllers exhibit a varying inverter frequency which causes undesirable harmonic heating and losses in the motor. A previous study provides a generic derivation of an adaptive bandwidth to minimize the frequency variation. In Chapter 2 of the thesis, this adaptive band theory is modified for application to a squirrel cage induction motor. Chapters 3 and 4 discuss the design and implementation of a complete prototype drive system incorporating the adaptive band control. Chapters 5 and 6 give results of simulations and laboratory tests which suggest that the developed control technique is successful in reducing inverter frequency variations, and thus in improving the overall performance of hysteresis band induction motor drives.

TABLE OF CONTENTS

CHAPTER	PAGE
1. INTRODUCTION	1
2. ADAPTIVE HYSTERESIS BAND CONTROL DERIVATION	6
3. CONTROL DESIGN	16
Direct Vector Control Method	19
Calculation of Rotor Flux, Emf, and Unit Vectors	21
Reference Current Vector Rotation and Differentiation	23
Adaptive HB Calculation Circuit	26
Comparator and Drive Circuit	29
4. HARDWARE CIRCUIT DESIGN	31
Analog Computer and ICs	32
Current Rotation and Differentiation Circuit	34
Flux, Emf, and Unit Vector Synthesis Circuit	36
Hysteresis Band Calculation Circuit	38
The Comparator Drive Circuit	40
Feedback Signal Processing Circuits	42
Power Circuit	44
5. SIMULATION STUDIES	47
Switching Frequency Determination	47
Hysteresis Band Simulation	49
Bandwidth Sensitivity to Leakage Inductance Variation	53

6. LABORATORY TEST RESULTS 58

Flux, Emf and Unit Vector Calculation 58

Vector Rotation and Current Differentiation Circuit 61

Hysteresis Band Calculation 62

Comparator and Drive Circuit 64

7. CONCLUSION 68

REFERENCES 69

VITA 71

LIST OF FIGURES

FIGURE		PAGE
2-1	Fixed HB PWM inverter control	7
2-2	Phase reference and actual current in HB controller	7
2-3	Current geometry in a hysteresis band	8
2-4	Inverter driven AC machine	10
2-5	Induction motor equivalent circuits	14
3-1	Adaptive HB PWM induction motor drive	17
3-2	Direct vector control principle	20
3-3	Flux, emf and unit vector estimation	24
3-4	Reference current rotation and differentiation	25
3-5	Hysteresis band control calculation	27
3-6	Fixed switching frequency determination	28
3-7	Transistor drive scheme	29
3-8	Comparator and drive circuit	30
4-1	Multiplier circuit configurations	33
4-2	Current rotation and differentiation circuit	35
4-3	Flux, emf and unit vector calculation circuit	37
4-4	Hysteresis band calculation circuit	39
4-5	Comparator and drive circuit	41
4-6	Current filter circuit	43
4-7	Frequency to voltage converter	44

4-8 Power circuit and inverter module 45

5-1 Hysteresis band simulation; no load; k = 0.667 51

5-2 Hysteresis band simulation; no load; k = 0.333 52

5-3 Band simulation with torque loading 54

5-4 Hysteresis band with decreased leakage inductance 56

5-5 Hysteresis band with increased leakage inductance 57

6-1 *d-q* axis flux signals 59

6-2 Phase *a* and *b* emf signals 60

6-3 Phase *a* emf and di^*/dt 60

6-4 Phase *a* and *b* reference currents 61

6-5 Phase *a* reference and differentiated current 62

6-6 Phase *a* hysteresis band and reference current 63

6-7 Comparator and drive circuit waveforms 65

6-8 Simulated motor phase current 67

CHAPTER 1

INTRODUCTION

The evolution of power electronics in recent decades has gradually given AC machines increased access to applications involving variable speed operation. DC machines have long been the more obvious choice in systems requiring a wide speed range, as accurate control is simply achieved by variation of the armature voltage and field current. Conventional synchronous and induction machine speeds, on the other hand, are tightly coupled to a normally constant supply voltage and frequency.

Methods in the past to vary AC machine speeds generally required additional motors, and were therefore costly and excessively bulky. An early Kramer Drive, for example, used two synchronous machines with a DC motor link to control the speed of one wound rotor induction machine. Other methods that did not involve the manipulation of either the supply voltage or frequency had significantly limited capabilities and were rarely implemented.

Today power electronics are widely used in converting power from fixed sources to clean variable voltage and frequency supplies. Although the cost and performance of power semiconductor devices have greatly improved since the invention of the thyristor, the initial cost of an AC machine and converter is still high. But these AC systems offer unsurpassed performance and reliability that generally result in lower operating and maintenance costs. The squirrel cage induction motor for example, when incorporated with static power conversion, has clear advantages over DC machines. Its short circuited

rotor consists of a single bar structure free of brushes, commutators, and insulation, thus permitting higher speed and temperature operation, with a greater power to weight ratio, and at a cost that is a fraction of an equivalently rated DC motor. Furthermore, the simple construction enables it to operate in environments that are too volatile for more elaborately built machines [1].

Methods of statically converting power for AC machine drives are numerous, but most fit into one of the following categories: Voltage fed inverters, current fed inverters, or phase controlled converters and cycloconverters [2]. Phase controlled converters, which use line commutation of switching devices, are popular for their simplicity. The stator voltage of an induction motor is controlled by adjusting the firing angle of the device relative to the supply voltage. The speed of the motor is then governed by the torque-speed curves over the range of stator voltages. Converters of this type induce poor line harmonics and are generally only preferred in low-power and low-performance applications. Most cycloconverters operate with the phase control principle to directly convert power from one voltage and frequency to another. Versatile thyristor control of both voltage and frequency made cycloconverters popular in early variable speed - constant frequency (VSCF) drives. The switching control is complex, however, and normally requires 18 or 36 thyristors for a three phase drive. This can be prohibitively expensive for all but very high power applications.

Current and voltage fed converters both incorporate an intermediate DC link between the supply and output AC; the former a stiff DC current, and the latter a stiff DC voltage. While offering some advantages, the current fed inverter is not generally

preferred over voltage fed inverters because of the large passive components required, slow control response, and poor performance at higher speeds [3]. Voltage fed converter schemes are the most popular for AC machine drives. They are the most versatile in terms of control configurations and types of acceptable devices. The simplest of these configurations is the square wave inverter. In this scheme, the transistors switch in fixed sequences to create a six-stepped voltage waveform at the desired frequency. Once again the trade off for simplicity here is performance. When operated at below rated speeds, undesirable low-order harmonics are created by the six-stepped waveform, and its applications are limited.

In recent years, pulse width modulation (PWM) control of voltage fed converters has come to be the standard for high performance drives in the low to medium power and speed ranges. PWM schemes switch devices many times during the cycle time of the fundamental frequency, controlling the output magnitude and frequency and limiting the low order harmonic content. One popular technique is sinusoidal PWM. This type uses the crossover points of a sinusoidal signal compared with a triangle carrier wave to control switching. The output waveform is controlled by varying the magnitude and frequency of the sine wave signal. Furthermore, maintaining the carrier frequency at specific multiples of the sine wave eliminates some unwanted harmonics.

Further harmonic reduction can be made using the harmonic elimination method, which creates notches in the voltage waveform at specified displacement angles. A constraint of these and other types of PWM methods is the commutation loss that occurs as a result of the inverter's high switching frequencies. Resonant link converter drives

have recently been developed which allow transistor switching only at the zero crossing of the voltage or current, thus eliminating commutation losses. These inverters, which use a resonant DC link, or series or parallel high frequency resonant links, show real promise in future machine drives.

Of the many types of PWM inverter systems, the hysteresis band (HB) current control technique offers some unique advantages. The combined use of a voltage fed inverter with current control means fast control loop response and peak device current limiting, the latter being especially important in transistor inverters. The current loop also prevents the DC link voltage ripple from adversely affecting control. Implementation of the HB inverter is also far easier than most other PWM methods. Control with a constant band requires no knowledge of most system parameters and is independent of most dynamic considerations. Its primary disadvantage is that the switching frequency may vary widely with a fixed hysteresis band, causing harmonic heating and losses in the machine. One simulation study showed how the switching frequency variations can be limited by modulating the hysteresis band according to system parameters. This study provided a generic bandwidth analysis and applied it to a permanent magnet machine in its simulation [4].

Despite the dependence on system parameters, the advantages of such a control scheme are numerous. Reducing the switching frequency bandwidth reduces the stator copper losses in the machine. Current subharmonics caused by frequency variations, and the resulting phase lag and dc offset in the fundamental wave with respect to the reference, can be reduced. The overall peak to peak current ripple can be reduced as

well, since a constant band must always be set for worst case operation. This would allow operation with higher steady state current ratings. Significant reductions in the current ripple would of course result a higher average switching frequency, and subsequently higher inverter loss. Therefore, optimum performance should be based on maintaining a balance of reduced switching frequency bandwidth and current ripple with a ceiling on the average switching frequency.

The thesis project presented here applies the adaptive HB method to a two horsepower squirrel cage induction motor in theory and in laboratory tests. A simulation study is made which considers the sensitivity of the calculated hysteresis band to varying parameters. The discussion includes development of the control design, practical considerations in its implementation, and a concluding analysis of the test results.

CHAPTER 2

ADAPTIVE HYSTERESIS BAND CONTROL DERIVATION

The hysteresis band PWM controller is a voltage fed inverter with current control. Reference currents i^*_a, i^*_b, and i^*_c are generated for a desired magnitude and frequency and compared with the actual machine currents. The resulting error is measured against a fixed prescribed hysteresis band, and the crossover points determine the switching pattern of the inverter (Figure 2-1). A phase current will rise with the upper leg transistor conducting, and upon touching the upper band, the bottom leg transistor will begin conducting causing the current to drop. Figure 2-2 shows the oscillating current within the prescribed band, which inspired the method's "bang bang control" nickname.

With a fixed bandwidth, the switching frequency varies over the fundamental cycle. Figure 2-2 gives a simplified depiction of how the switching frequency increases at the positive and negative peaks, while dropping low near the zero crossings where the slope of the reference current is high. By modulating the hysteresis band then, the switching frequency variations can be limited, thereby reducing the amount of harmonic heating and losses in the machine. The adapting band can be calculated as a function of the switching frequency, inverter voltage, counter electromotive force (emf) and other factors which determine the behavior of the current.

The following bandwidth derivation, for an AC machine with counter emf and an unconnected neutral, has been developed by B. K. Bose[4], but is repeated here for thoroughness. Then, this derivation is applied to a squirrel cage induction motor.

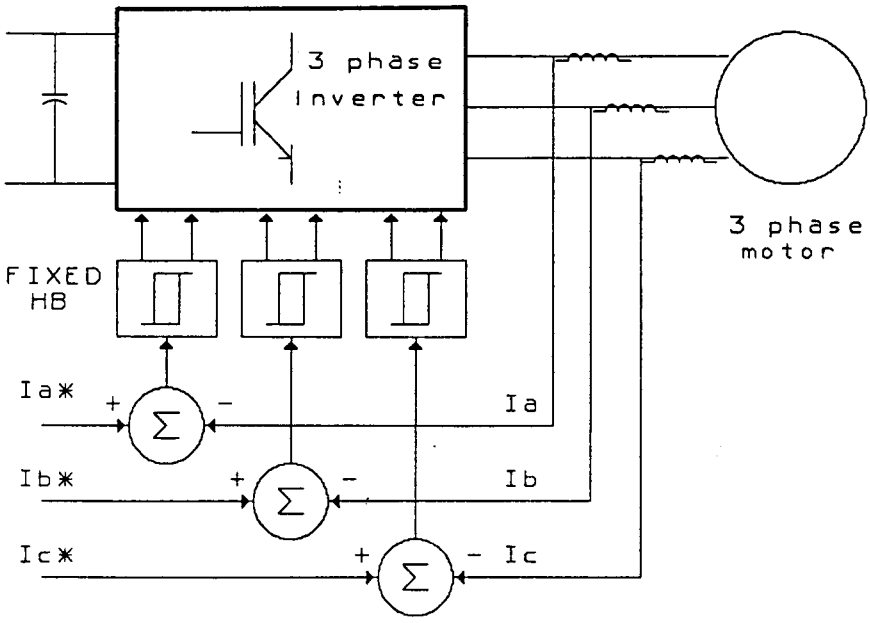


Figure 2-1: Fixed HB PWM inverter control

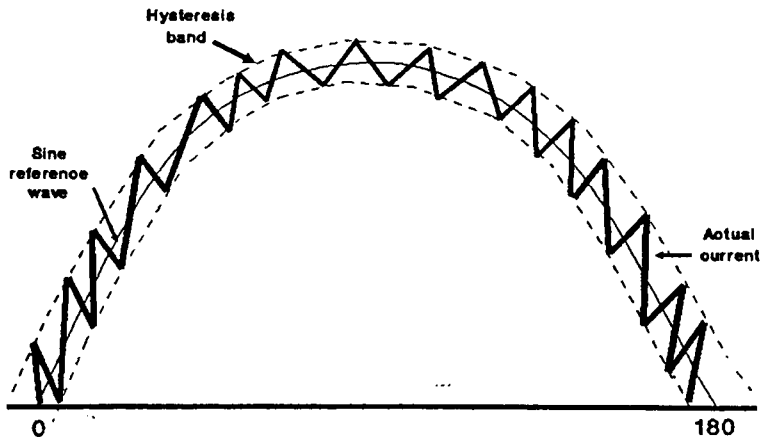


Figure 2-2: Phase reference and actual current in HB controller

A geometric analysis of Figure 2-3 shows that the hysteresis band of a single phase can be described by

$$2HB = \frac{di^+}{dt} t_1 - \frac{di^*}{dt} t_1 \tag{2.1}$$

and

$$-2HB = \frac{di^-}{dt} t_2 - \frac{di^*}{dt} t_2 \tag{2.2}$$

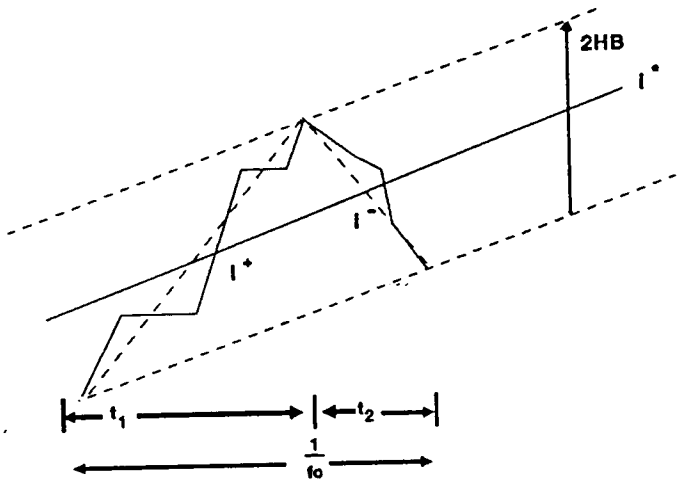


Figure 2-3: Current geometry in a hysteresis band

Adding (2.1) and (2.2) gives

$$\frac{di^+}{dt} t_1 + \frac{di^-}{dt} t_2 - \frac{di^*}{dt} (t_1 + t_2) = 0 \tag{2.3}$$

or,

$$\frac{di^+}{dt} t_1 + \frac{di^-}{dt} t_2 - \frac{di^*}{dt} \frac{1}{f_c} = 0 \tag{2.4}$$

where

$$t_1 + t_2 = T_c = \frac{1}{f_c} \tag{2.5}$$

Furthermore, subtracting (2.2) from (2.1) gives

$$\frac{di^+}{dt} t_1 - \frac{di^-}{dt} t_2 - \frac{di^*}{dt} (t_1 - t_2) = 4HB \tag{2.6}$$

To apply this to an AC machine, it is first necessary to analyze the current behavior when the machine is supplied by an inverter with an unconnected neutral. Figure 2-4 shows the inverter driving the machine, which is represented by an inductor connected in series to an emf (V_f) source for each phase. The machine phase to neutral voltages are given by

$$V_{an} = \frac{2}{3} V_{a0} - \frac{1}{3} (V_{b0} + V_{c0}) \tag{2.7}$$

$$V_{bn} = \frac{2}{3} V_{b0} - \frac{1}{3} (V_{a0} + V_{c0}) \tag{2.8}$$

$$V_{cn} = \frac{2}{3} V_{c0} - \frac{1}{3} (V_{a0} + V_{b0}) \tag{2.9}$$

since

$$V_n = \frac{1}{3} (V_{a0} + V_{b0} + V_{c0}) \tag{2.10}$$

The voltage in each phase therefore is dependent on the switch positions of the other phases. As a result, when transistor T_1 is conducting, the voltage in phase *a* may be *0*, $V_d/3$, or $2V_d/3$, where V_d is the inverter DC link voltage. Table 2-1 shows the possible combinations of transistor conduction and the corresponding voltage for phase *a*. Since the positive and negative voltages in each phase are somewhat randomly distributed as $V_d/3$ or $2V_d/3$, the value will henceforth be referred to as $-kV_d$ or kV_d. In the actual control algorithm, *k* will be varied between *1/3* and *2/3* to minimize the switching frequency bandwidth.

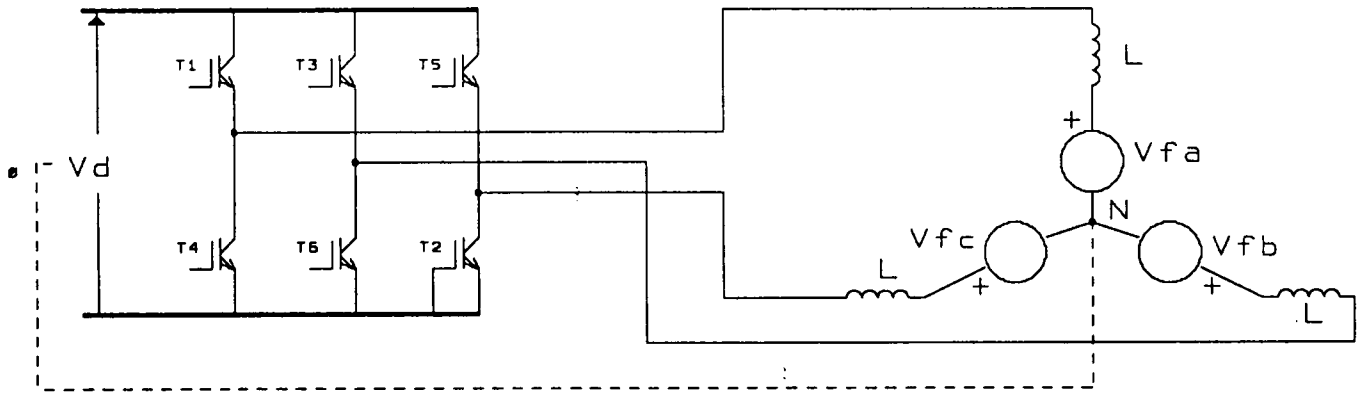


Figure 2-4: Inverter driven AC machine

Table 2-1: Transistor Conduction and Phase *a* Voltage

Conducting Device			Voltage Phase *a*
T_1	T_6	T_2	2/3 V_d
T_1	T_6	T_5	1/3 V_d
T_1	T_3	T_2	1/3 V_d
T_1	T_3	T_5	0
T_4	T_3	T_5	-2/3 V_d
T_4	T_3	T_2	-1/3 V_d
T_4	T_6	T_5	-1/3 V_d
T_4	T_6	T_2	0

Now, the voltage and current relation in an HB controlled inverter drive can be given. The current rise in a single phase is

$$\frac{di^+}{dt} = \frac{1}{L}(kV_d - V_f) \tag{2.11}$$

and the dropping current is

$$\frac{di^-}{dt} = -\frac{1}{L}(kV_d + V_f) \tag{2.12}$$

Here V_f is the phase emf seen by the stator, and L is the motor leakage inductance. The voltage drop across the stator resistance is considered negligible. For purposes of calculation, an assumption is also made that the voltages do not change appreciably during a switching cycle.

Note that the voltages are subtractive when the inverter upper leg is conducting and additive when the bottom leg is conducting. For a given switching period and typical emf, then, the current drop in the band will be faster than the current rise. In fact, in a period of current rise t_1, the current slope will temporarily become negative if the value of kV_d is less than the emf voltage. In a period of current drop t_2, on the other hand, the

slopes will vary in magnitude, but will almost always be negative. More discussion of this phenomenon will be given later.

Substituting equations (2.11) and (2.12) into (2.4) gives

$$(kV_d - V_f)\frac{t_1}{L} - (kV_d + V_f)\frac{t_2}{L} - \frac{di^*}{dt}\frac{1}{f_c} = 0 \qquad (2.13)$$

Equation (2.13) simplifies to

$$\frac{kV_d}{L}(t_1 - t_2) - \frac{V_f}{L}\frac{1}{f_c} - \frac{di^*}{dt}\frac{1}{f_c} = 0 \qquad (2.14)$$

Therefore,

$$t_1 - t_2 = \frac{L}{kV_d f_c}\left(\frac{V_f}{L} + \frac{di^*}{dt}\right) \qquad (2.15)$$

Now, substituting equations (2.11), (2.12) and (2.15) into (2.6) gives

$$4HB = (kV_d - V_f)\frac{t_1}{L} + (kV_d + V_f)\frac{t_2}{L} - \frac{di^*}{dt}\frac{L}{kV_d f_c}\left(\frac{V_f}{L} + \frac{di^*}{dt}\right) \qquad (2.16)$$

or,

$$HB = \frac{kV_d}{4L}(t_1 + t_2) - \frac{V_f}{4L}(t_1 - t_2) - \frac{di^*}{dt}\frac{L}{4kV_d f_c}\left(\frac{V_f}{L} + \frac{di^*}{dt}\right) \qquad (2.17)$$

so

$$HB = \frac{kV_d}{4f_c L} - \frac{di^*}{dt}\frac{2V_f L}{4LkV_d f_c} - \frac{L}{4kV_d f_c}\left[\left(\frac{V_f}{L}\right)^2 + \left(\frac{di^*}{dt}\right)^2\right] \qquad (2.18)$$

i.e.

$$HB = \frac{kV_d}{4f_c L} - \frac{L}{4kV_d f_c}\left(\frac{V_f}{L} + \frac{di^*}{dt}\right)^2 \qquad (2.19)$$

or

$$HB = \frac{kV_d}{4f_c L}\left[1 - \frac{L^2}{k^2 V_d^2}\left(\frac{V_f}{L} + \frac{di^*}{dt}\right)^2\right] \tag{2.20}$$

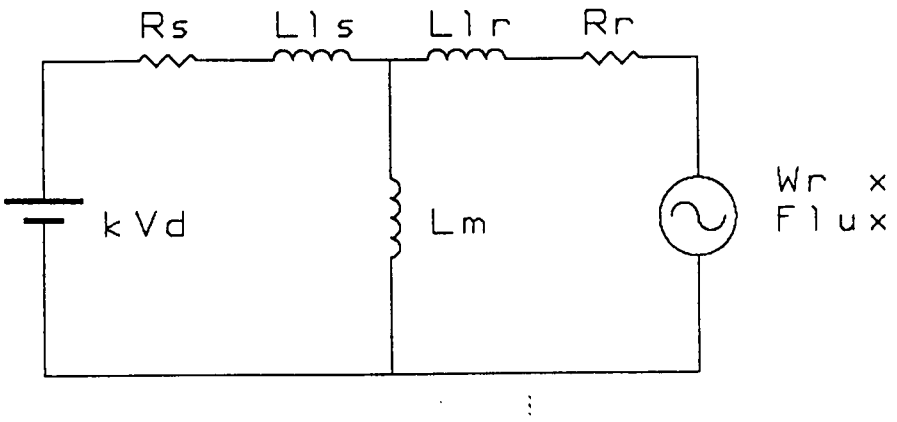
To apply this derivation specifically to an induction motor, a method of determining the emf in each phase that can be practically implemented must be devised. Figure 2-5 shows a per phase equivalent circuit representation of an induction motor. In Figure 2-5a, the counter emf is in phase with the rotor flux. In Figure 2-5b, the magnetizing inductance is assumed large, and the stator and rotor resistances and inductances are combined into Thevenin equivalent values. The resulting approximation of the counter emf as seen by the stator is the product of the rotor speed in radians per second and the phase rotor flux [5].

$$V_f = \omega_r \times \psi_r \tag{2.21}$$

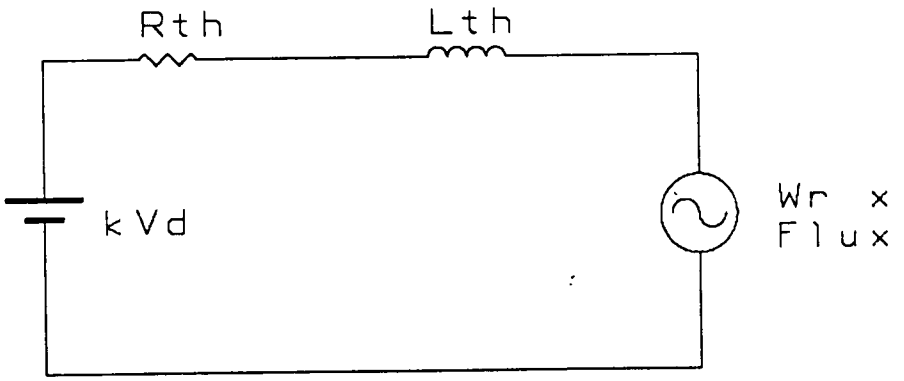
The hysteresis band for a single phase is now given by

$$HB = \frac{kV_d}{4f_c L}\left[1 - \frac{L^2}{k^2 V_d^2}\left(\frac{\omega_r \psi_r}{L} + \frac{di^*}{dt}\right)^2\right] \tag{2.22}$$

Equation (2.22) reveals the dependent nature the hysteresis band and similarly the switching frequency has on the various system parameters. During constant band operation at slow speeds, the switching frequencies tend to reach undesirably high levels [6]. With the modulating band however, the relation to the square of the current reference wave serves to correct this problem.



a: Induction motor equivalent circuit



b: Simplified equivalent circuit

Figure 2-5: Induction motor equivalent circuits

Analysis at higher speeds and emf becomes more complicated. A high emf in most instances serves to reduce the voltage across the inductor and reduce the switching frequency. The phase relation of the emf and the reference current may in some cases, however, result in additive voltages causing a high *di/dt* at a point when the hysteresis band is minimum. Also, Honsinger [7] has shown that the effective inductance in an inverter driven induction machine may drop significantly with higher speeds. A dropping inductance has a drastic effect on the size of the hysteresis band as well as the current slopes. The sensitivity of these various parameters will be further addressed in Chapter 5.

CHAPTER 3

CONTROL DESIGN

A detailed discussion of the control design of an entire adaptive hysteresis band motor drive system is given in this chapter. The block diagram in Figure 3-1 shows the overall control scheme and the various subsystems. The description of the drive subsystems and the control topology is summarized as follows:

- The Direct Vector Method of Control

The system incorporates direct vector or field control, which requires feedback parameters and axis transformation of the current and flux signals. Vector control enables AC machines to be controlled similar to DC machines, where the field and torque commands are decoupled.

- Flux, Emf, and Unit Vector Synthesis

Rotor flux and emf and line frequency unit vectors are synthesized based on calculations that are a function of the machine line currents, rotor speed, and motor resistive and inductive parameters [5].

- Vector Rotation and Differentiation of Reference Currents

This circuit inputs the unit vectors and dc command signals to generate the reference currents and differentiated reference currents for the comparator and HB calculation circuits respectively.

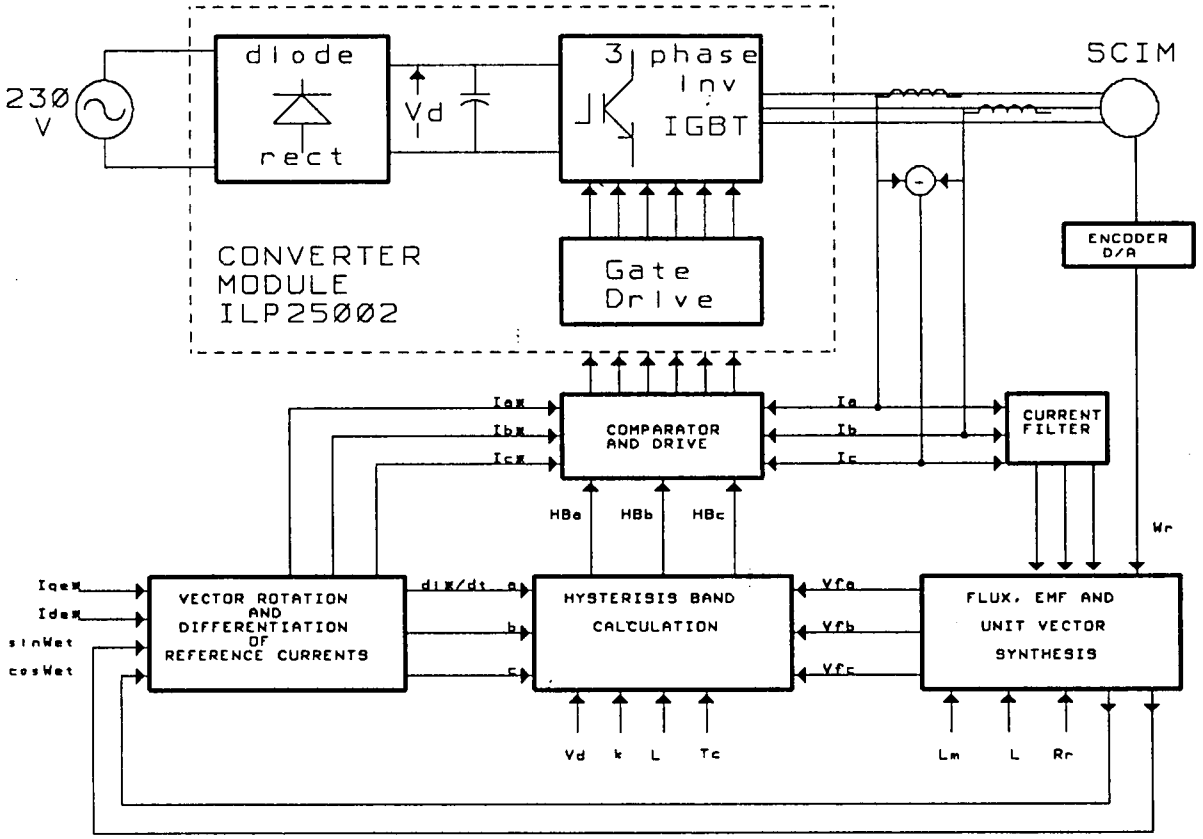


Figure 3-1: Adaptive HB PWM induction motor drive

- Hysteresis Band Calculation

This circuit receives the required parameter values and calculates three phase adaptive bands for the comparator drive circuit.

- Comparator and Drive Design

The reference and actual currents are compared with the generated hysteresis bands and processed for control of the inverter gate drive.

The power circuit includes an integrated converter module and a two horsepower induction motor, the details of which will be discussed in Chapter 4, which describes the hardware design. Calculations of the hysteresis bands, counter emf signals, reference currents and differentiated reference currents are all performed in real time by an analog computer interfaced with exterior analog integrated circuits. While somewhat bulky and outdated, an analog computer provides excellent control loop response. The machine currents are measured with current transformers and are used directly in the comparator circuit. They are also filtered for use in the flux synthesis circuit. The machine rotor speed is measured using an optical encoder attached to the motor and is converted to a DC voltage for use in the flux and emf calculations. While the type of encoder used in this system is attached to the end of the shaft and prevents torque loading, other types of encoders can be mounted around the shaft, eliminating this limitation. The overall control scheme is designed for steady state operation in the constant torque speed range of the motor.

3.1 Direct Vector Control Method

The direct vector method of control was introduced by F. Blaschke [5] in the early 1970s as a means to provide decoupled control of AC machines. This method entails the conversion of three-phase currents and flux signals to a two-phase direct and quadrature (*d-q*) axis. If the *d-q* axis as a reference frame is rotating at synchronous speed, the current components i_{qe} and i_{de} become analogous to the armature and field currents, respectively, in a DC machine. As command signals, the *d-q* currents therefore provide decoupled control of the field and torque, which in turn improve control response. The term direct means that unit vectors are generated from direct measurement of machine signals.

Figure 3-2 shows the direct vector control method as it applies to this project. Machine output currents and speed are used to estimate the rotor flux and then calculate the unit vectors $sinw_e t$ and $cosw_e t$. These vectors are factored in with the input *d-q* current commands and transformed to produce the three-phase reference currents.

The measured machine stator currents are first converted to a two-phase stationary axis defined by

$$i_{qs} = i_a \tag{3.1}$$

and

$$i_{ds} = -\frac{1}{\sqrt{3}} i_b + \frac{1}{\sqrt{3}} i_c \tag{3.2}$$

to calculate flux and unit vectors.

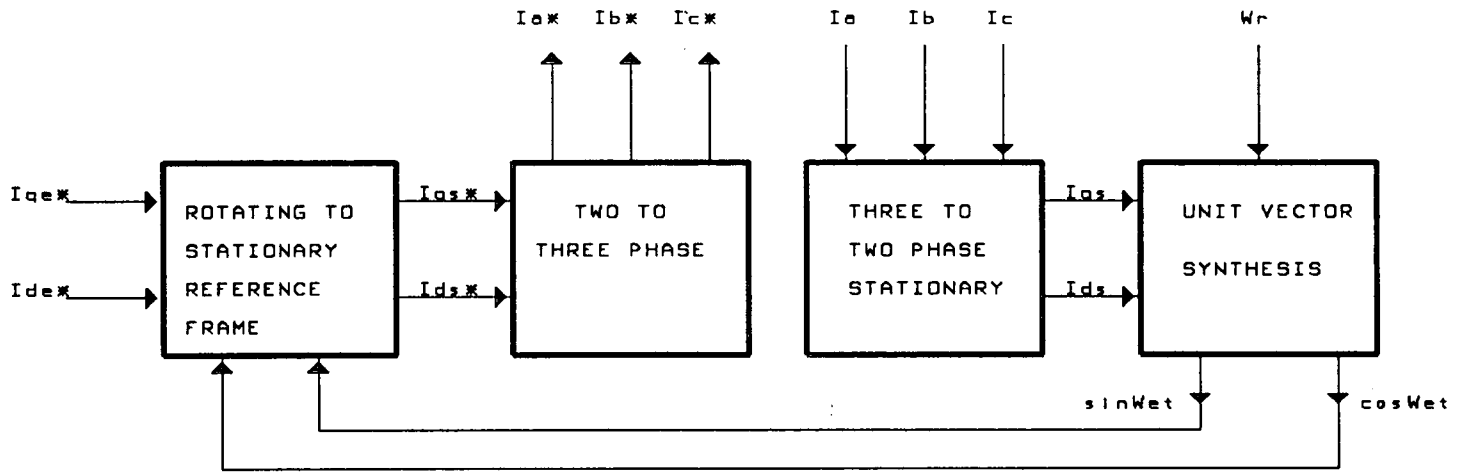


Figure 3-2: Direct vector control principle

On the command side, the rotating axis DC current components are converted to two-phase stationary (sinusoidal) components using the unit vectors.

$$i_{qs}^* = i_{qe}^* \cos\omega_e t + i_{de}^* \sin\omega_e t \tag{3.3}$$

$$i_{ds}^* = -i_{qe}^* \sin\omega_e t + i_{de}^* \cos\omega_e t \tag{3.4}$$

The stationary components are converted back to three-phase reference currents by

$$i_a^* = i_{qs}^* \tag{3.5}$$

$$i_b^* = -\frac{1}{2} i_{qs}^* - \frac{\sqrt{3}}{2} i_{ds}^* \tag{3.6}$$

and

$$i_c^* = -\frac{1}{2} i_{qs}^* + \frac{\sqrt{3}}{2} i_{ds}^* \tag{3.7}$$

The direct vector control method is especially attractive for this system. Estimating the rotor flux establishes a ready means of calculating the counter emf, which is used in determining the hysteresis band. Similarly, the differentiated reference currents can be generated algebraically in the vector rotation circuit.

3.2 Calculation of Rotor Flux, Emf, and Unit Vectors

Flux and unit vector calculations are made using feedback current and rotor speed signals. In this case, the rotor flux as opposed to the air gap flux is estimated because the method is more reliable at lower speeds. The measured currents are filtered to reduce harmonic distortion in the calculated waveforms. Care must be taken in designing

a filter so that any phase shift introduced is insignificant. Once filtered, the currents are transformed to stationary *d-q* axis components. The *d-q* rotor fluxes in an induction motor are given by

$$\psi_{qr} = \int \left(\frac{L_m}{T_r} i_{qs} + \omega_r \psi_{dr} - \frac{1}{T_r} \psi_{qr} \right) dt \tag{3.8}$$

and

$$\psi_{dr} = \int \left(\frac{L_m}{T_r} i_{ds} - \omega_r \psi_{qr} - \frac{1}{T_r} \psi_{dr} \right) dt \tag{3.9}$$

where $T_R = L_R / R_R$, the rotor resistance and inductance.

Since these fluxes are referenced to the stationary axis, they rotate at synchronous speed with 90 degree displacement. Therefore the unit vectors $sinw_e t$ and $cosw_e t$ can be calculated as

$$\sin\omega_e t = \frac{\psi_{qr}}{\sqrt{\psi_{qr}^2 + \psi_{dr}^2}} \tag{3.10}$$

and

$$\cos\omega_e t = \frac{\psi_{dr}}{\sqrt{\psi_{qr}^2 + \psi_{dr}^2}} \tag{3.11}$$

In Chapter 2, it was shown that the phase counter emf of an induction motor can be approximated by

$$V_f = \omega_r \psi_r \tag{3.12}$$

The *d-q* axis rotor fluxes can be converted to three-phase by the same method used for the currents in equations (3.5), (3.6), and (3.7). Multiplying these fluxes by the rotor speed then gives the approximate three-phase emf voltages.

$$V_{fa} = \omega_r \psi_{ar} = \omega_r \psi_{qr} \tag{3.13}$$

$$V_{fb} = \omega_r \psi_{br} = \omega_r \left(-\frac{1}{2} \psi_{qr} - \frac{\sqrt{3}}{2} \psi_{dr} \right) \tag{3.14}$$

and

$$V_{fc} = \omega_r \psi_{cr} = \omega_r \left(-\frac{1}{2} \psi_{qr} + \frac{\sqrt{3}}{2} \psi_{dr} \right) \tag{3.15}$$

Figure 3-3 shows a block diagram of the calculations made in this circuit, including the three- to two-phase current transformation.

3.3 Reference Current Vector Rotation and Differentiation

In the vector rotation circuit shown in Figure 3-4, reference currents are transformed from the rotating *d-q* axis to three-phase command currents as described in Section 3.1. However, differentiated reference currents are also required for the calculation of the adaptive hysteresis bands. These can be calculated as functions of the *d-q* currents. Taking the derivative of the stationary axis currents given in equations (3.3) and (3.4) with respect to time gives

$$\frac{di_{qs}^*}{dt} = \omega_e \left(i_{de}^* \cos\omega_e t - i_{qe}^* \sin\omega_e t \right) \tag{3.16}$$

and

$$\frac{di_{ds}^*}{dt} = \omega_e \left(-i_{qe}^* \cos\omega_e t - i_{de}^* \sin\omega_e t \right) \tag{3.17}$$

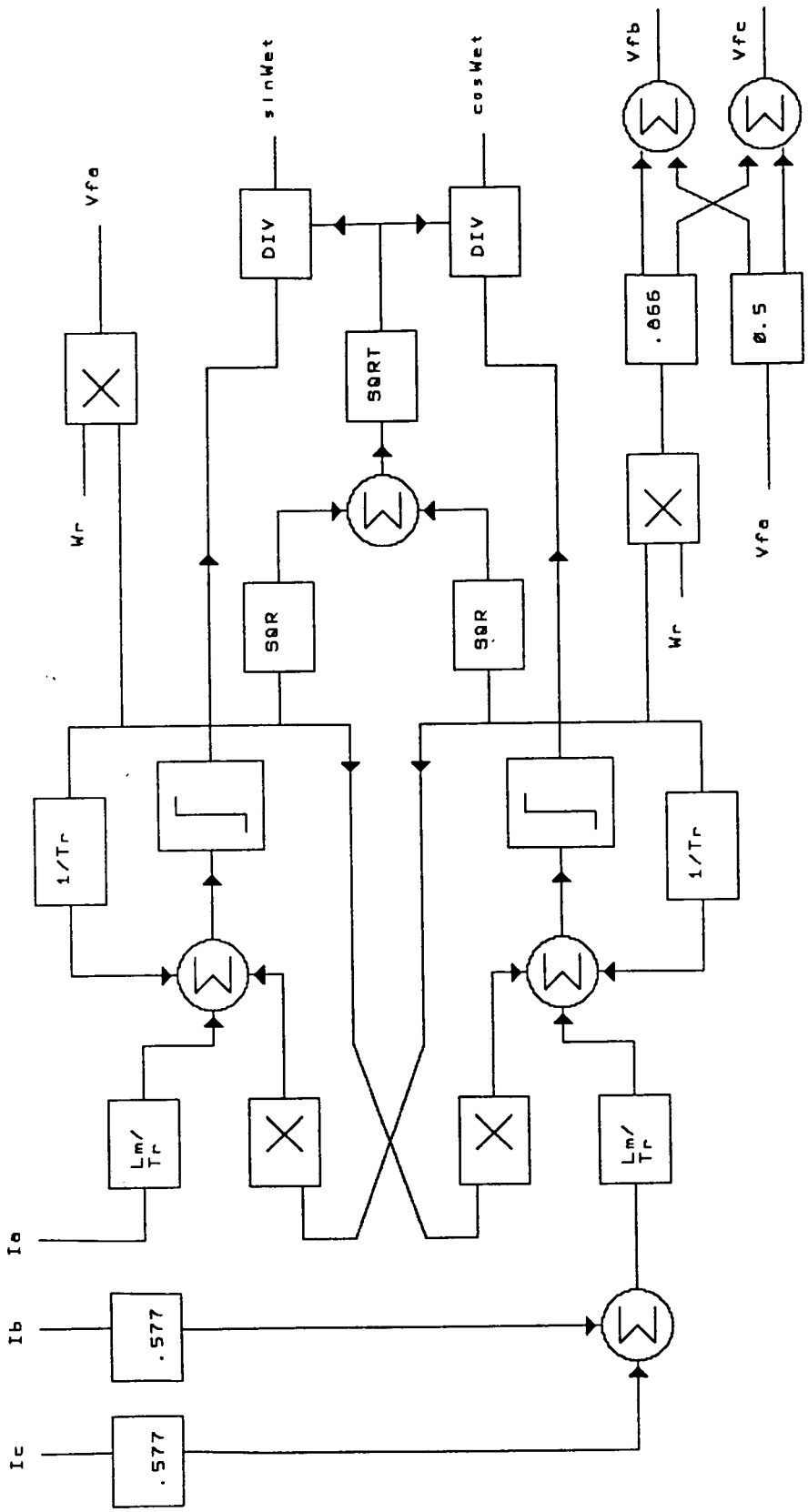


Figure 3-3: Flux, emf and unit vector estimation

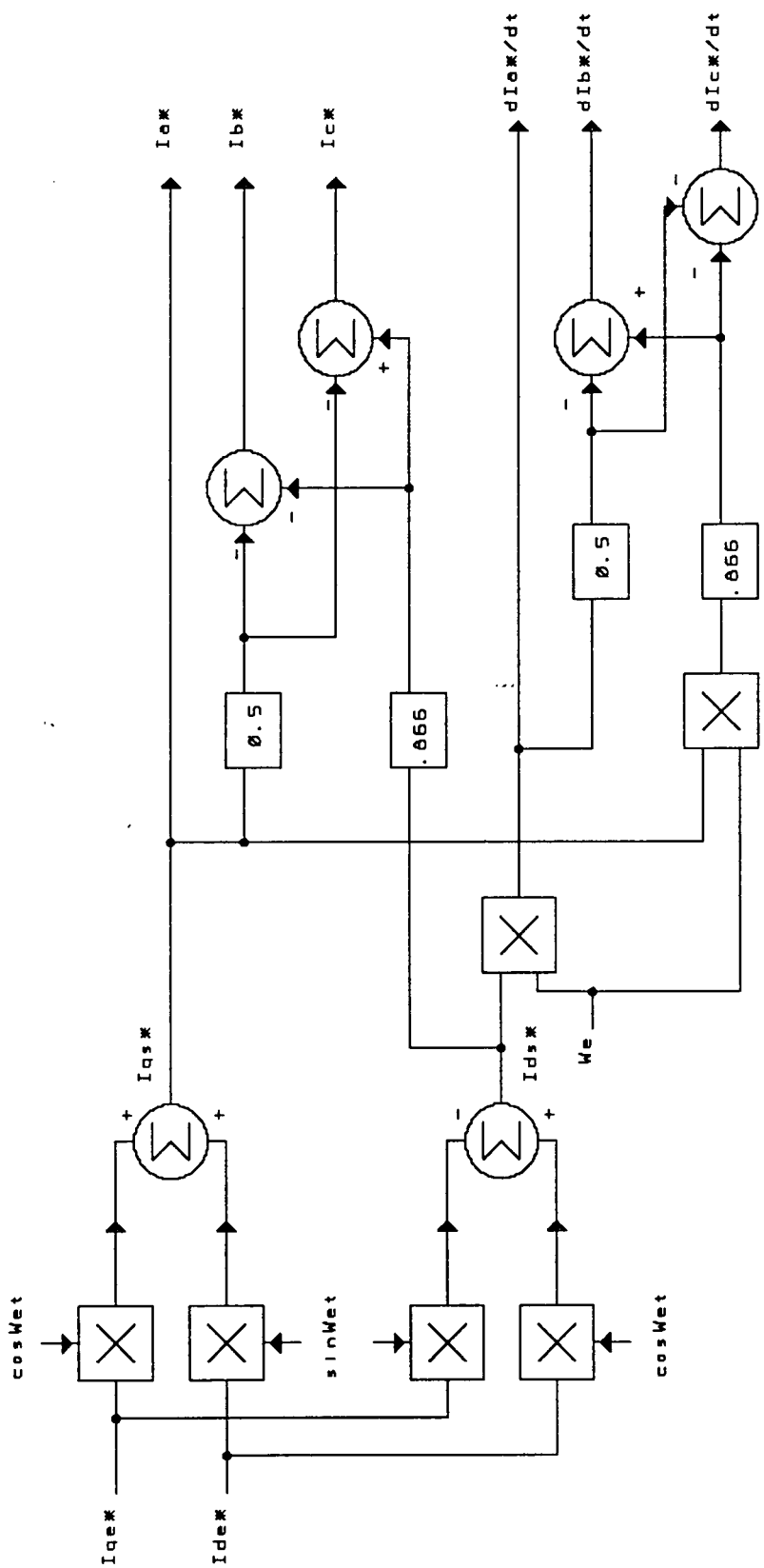


Figure 3-4: Reference current rotation and differentiation

Combining (3.16) and (3.17) with (3.5), (3.6) and (3.7) gives the three phase differentiated reference currents.

$$\frac{di_a^*}{dt} = \omega_e i_{ds}^* \tag{3.18}$$

$$\frac{di_b^*}{dt} = \omega_e\left(-\frac{1}{2} i_{ds}^* + \frac{\sqrt{3}}{2} i_{qs}^*\right) \tag{3.19}$$

and

$$\frac{di_c^*}{dt} = \omega_e\left(-\frac{1}{2} i_{ds}^* - \frac{\sqrt{3}}{2} i_{qs}^*\right) \tag{3.20}$$

Note that these currents are only valid during steady state operation since it is assumed that w_e is constant. Transient operation would require the additional consideration of the change in w_e with respect to time.

3.4 Adaptive HB Calculation Circuit

The single phase modulating hysteresis band in equation (2.22) is a function of the following parameters:

V_d	The inverter DC link voltage
di^*/dt	The differentiated reference current
f_c^*	The average switching frequency
V_f	The counter emf calculated from the flux and rotor speed w_r
L	The leakage inductance

Figure 3-5 shows the control diagram for the three-phase hysteresis band calculation.

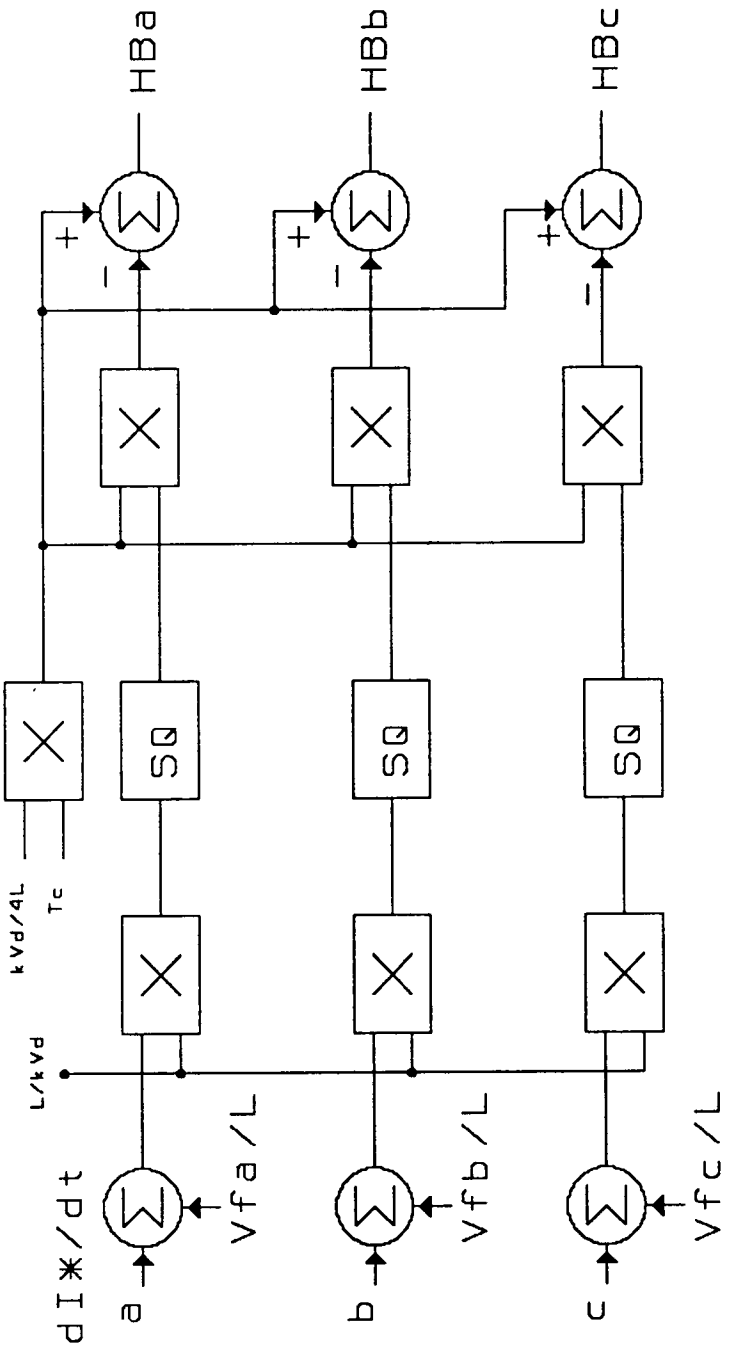


Figure 3-5: Hysteresis band control calculation

Although the actual value of f_c will vary during operation, a fixed value f_c^* should be used in the calculation of *HB*. This is to prevent unwanted distortion of the *HB* waveform relative to the reference currents. The value of f_c^* is approximated for start up and then is altered based on visual monitoring of a transistor base drive signal which is converted in a frequency to voltage circuit. The fixed switching frequency is the median value of the observed actual frequency, as shown in Figure 3-6.

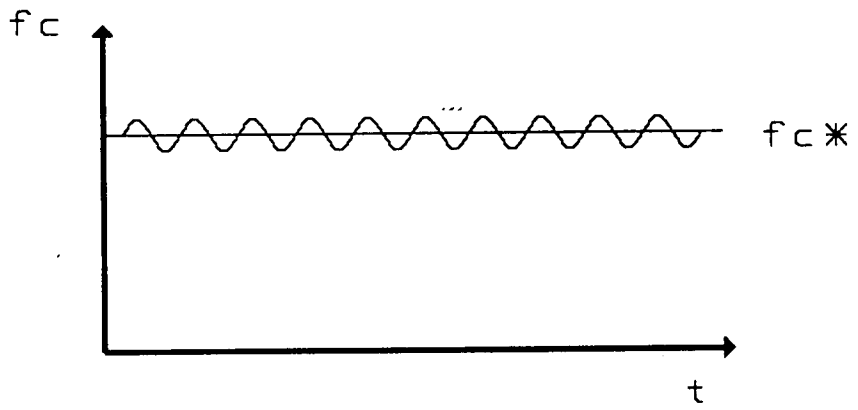


Figure 3-6: Fixed switching frequency determination

The variable *k*, recalling from Chapter 2, represents a value ranging from *1/3* to *2/3*. This is set conservatively (i.e. > *2/3*) during start up, and then gradually reduced. The optimum setting is based on minimizing the bandwidth of the actual switching frequency f_c about f_c^*, while preventing the average frequency from getting too high. Minimizing the frequency bandwidth is essential for minimizing the current harmonic content and machine losses.

3.5 Comparator and Drive Circuit

The comparator circuit provides the inverter drive signals according to comparisons of the actual and reference currents with the calculated hysteresis band. Base drive signals as a function of the three input signals are given as follows for a single phase of the inverter, shown in Figure 3-7.

$$T1 \text{ conducts when } i_a^* - HB - i_a > 0$$

$$T4 \text{ conducts when } i_a - HB - i_a^* > 0$$

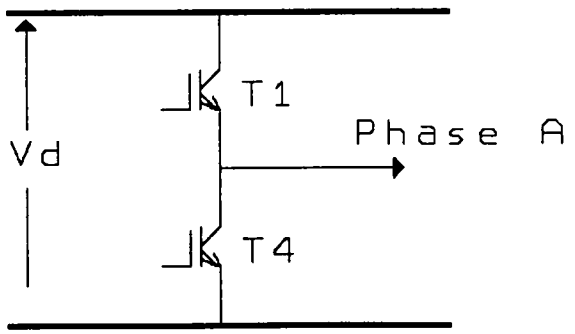


Figure 3-7: Transistor drive scheme

The current behavior in a single phase is also dependent on the currents of the other two phases. As was discussed in Chapter 2, the slopes of the rising and falling currents may approach zero or temporarily become negative as a result of switching in the other phases. A comparison of a sloping current with respect to the hysteresis band may have difficulties if the *relative* slope is small. As an added caution then, a one shot device is designed into the circuit to prevent any oscillations that might occur from a slow comparator zero crossing. The one shot sets a minimum pulsewidth for the drive signal.

Figure 3-8 shows the comparator circuit design for one phase. The flip flop circuit latches when a pulse from the *T1* comparator is received. *T1* subsequently stays on until a pulse from the *T4* comparator is received at the *S* input. When this occurs the signal to *T1* goes off and *T4* goes on. The lock out circuit, which prevents both transistors from conducting simultaneously, is contained in the power module gate drive.

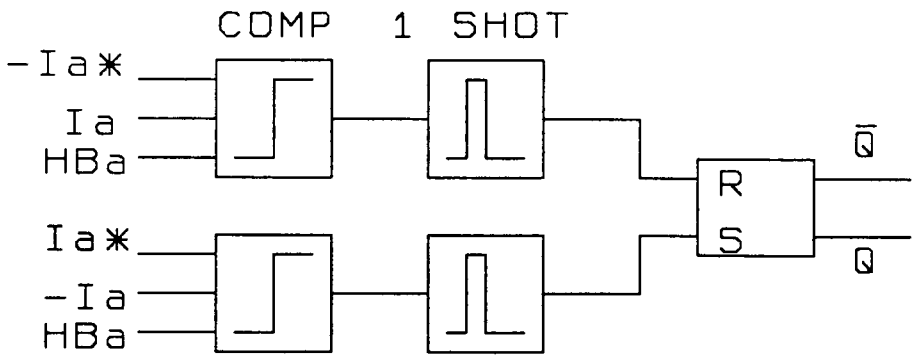


Figure 3-8: Comparator and drive circuit

CHAPTER 4

HARDWARE CIRCUIT DESIGN

This chapter discusses the development of a laboratory prototype hysteresis band PWM induction motor drive based on the control design described in Chapter 3. The main components include:

- A 2 horsepower cage induction motor and encoder
- A power rectifier-IGBT inverter module and gate drive
- An analog computer
- Supporting analog and digital integrated circuitry

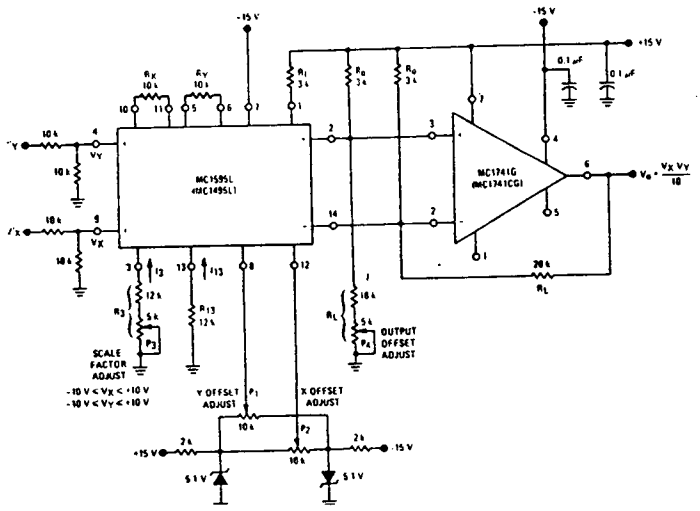
While many of the analog computations are made on the computer, additional analog integrated circuits (ICs) are necessary. Development of a scaling system based on no load operation at 30 Hz is discussed in detail for each subsystem described in Chapter 3. Digital components are also used in the comparator and frequency to voltage (f-V) conversion circuits. Each subsystem was built and tested separately before combining them as a whole. The testing was performed by simulating the actual operation in each subsystem, using inputs representing expected real signals. Feedback processing and control loop circuits were tested using a separate PWM inverter to drive the motor. While this system was developed mainly with available components and convenience in mind, its implementation is not limited to analog hardware. Its functions can easily be performed by microcomputer drives.

4.1 Analog Computer and IC Circuits

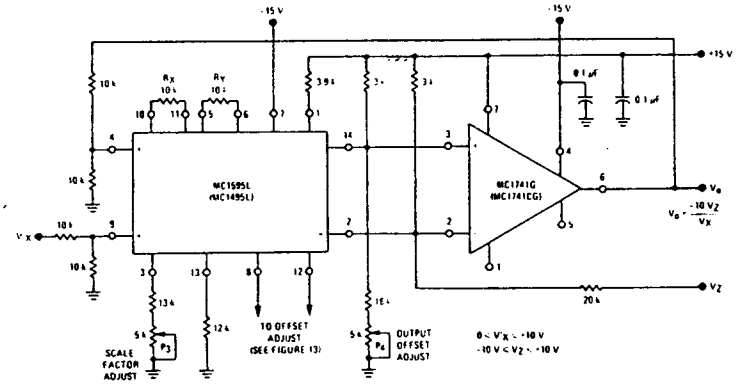
Since the number of analog computation components necessary for the control system exceed those available on the computer, supporting analog IC circuits are incorporated. The complete analog system includes the computer, 15 multiplier and support ICs and twenty interface lines.

The computer is an EAI 681 Parallel Analog Processor [8]. Along with the summers, multipliers and integrators, the computer contains inverters, potentiometers and trunk terminals for interfacing with external components. Connections of the internal components are made on an external patch panel. The potentiometers and amplifiers outputs are all accessible by a digital readout panel controlled by a keyboard. Scale settings for the potentiometers are also made with the keyboard. All of the amplifiers have a plus and minus 10 volt output range; scaling of the various parameters is required.

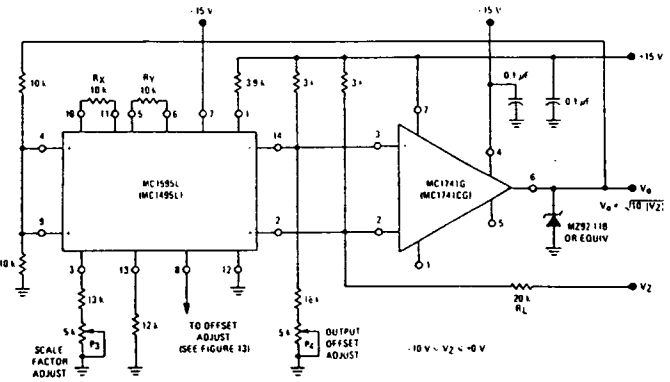
The analog IC components are put together on a breadboard and interfaced with the computer via the trunk lines. The devices used for multiplication, division and square root functions are Motorola MC1495 and MC1595 four-quadrant multipliers [9]. The MC1595 is a higher precision device used in the divide and square root circuits, which are inherently less accurate than the multiply circuits. Because calculations made for both the hysteresis band and flux estimation are very sensitive to drift and DC offset, each multiplier circuit (for all functions) includes offset adjustment potentiometers and an op-amp output to control level shift. Figure 4-1 shows the design diagrams of the three types of circuit functions used. The scale factor and x and y offset adjustments can be set permanently, but the output offset is left variable because drift sometimes occurs



a: Multiply circuit



b: Divide circuit



c: Square Root Circuit

Figure 4-1: Multiplier circuit configurations

during system start up. Individual IC scaling is achieved using the equation

$$k_1 = \frac{2R_L}{R_x R_y I_3} \tag{4.1}$$

with the values shown in the figure. The resistors R_x and R_y are fixed, so fine adjustments are made using a potentiometer to control I_3. The inherent scale range for these multipliers is from about 1/10 to 4/10, so additional scaling requires voltage dividers at the inputs or outputs.

4.2 Current Rotation and Differentiation Circuit

Figure 4-2 shows the reference current transformation and differentiation circuit. The calculations for this circuit are performed entirely on the computer. In the figure, the summers appear with op-amp notation, and the inverters are given by their standard digital notation. Each summer has an inverted output and unity or times 10 gain capability. The *x, y* squares are multipliers, which are 1/10 gain and have inverting or non-inverting output capability. The circles represent potentiometers and the open junction symbols, here denoted by *T10* and *T11*, are trunk terminals input from external hardware. The numbers on the various components denote the amplifier number on the computer associated with each function. Here the circuit performs the functions described in Section 3.3. Unit vectors $sinw_e t$ and $cosw_e t$ are input via the trunks from the flux estimation circuit. I_{qe}^* and I_{de}^* are the DC torque and flux components respectively that are used for decoupled control of the motor. These are hand set using the potentiometers.

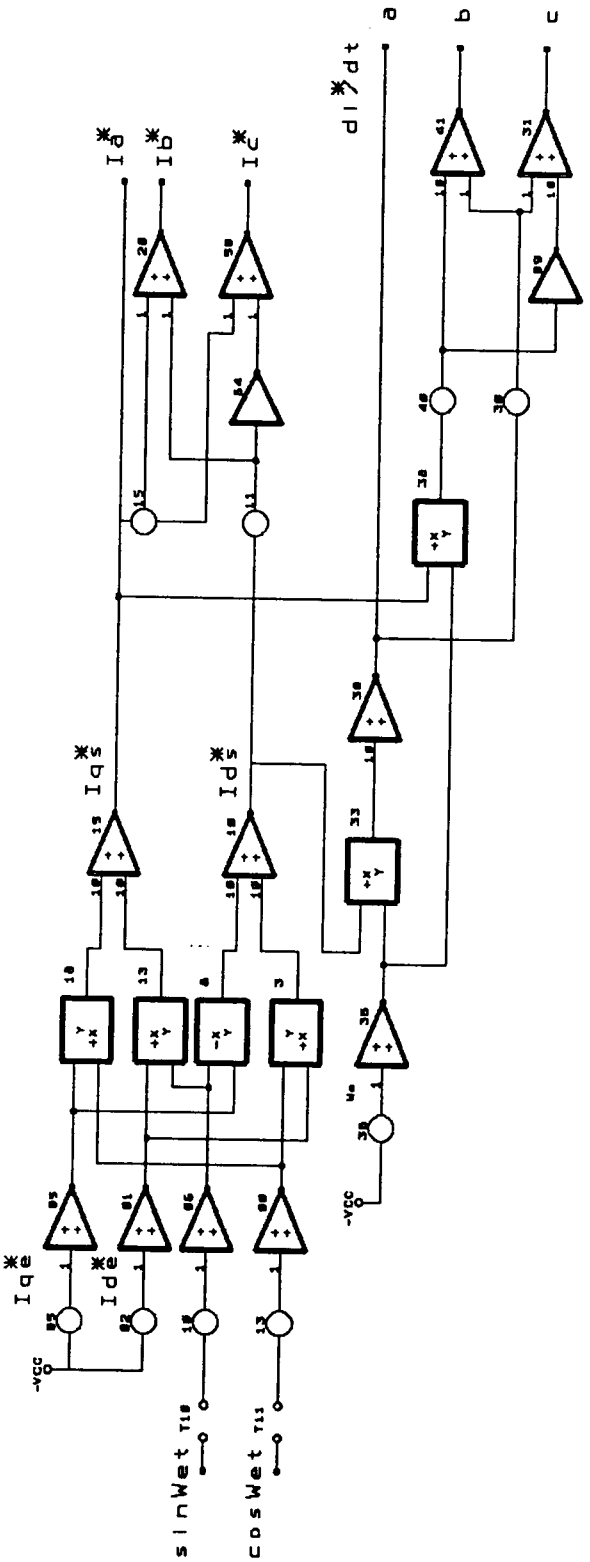


Figure 4-2: Current rotation and differentiation circuit

Early testing of the motor under no load conditions showed that the current required for 30 Hz operation was about 5 amps 0-peak. The currents in this section and all others then are scaled 1 volt = 1 amp. I_{qe}^* and I_{de}^* are set equally at 4 volts for testing, which generates 5 volt (0-peak) reference current signals. The synchronous angular frequency w_e is a command signal set for 30 Hz or 189 radians per second. The scale of w_e is 1 volt = 200 rad/sec, so it has a 30 Hz voltage value of 0.95. The figure shows some of the summers using gain 10 inputs, which in this case result from following multipliers which are 1/10 gain. The reference current outputs are unity gain inputs to the comparator circuits, while the *di/dt* outputs have a gain of 1/200, due to factoring with w_e. These are further reduced by a factor of 10 before adding with the emf current component in the hysteresis band calculation circuit.

4.3 Flux, Emf, and Unit Vector Synthesis Circuit

This circuit combines the computer with some of the external analog hardware. The circuit diagram shown in Figure 4-3 denotes the IC circuits, which are labeled by their function and part numbers MC1495, MC1595, or OP27 op amps. Computer amps 65 and 95 are integrators, carrying the standard analog notation. The circuit inputs unity gain (1 volt = 1 amp) stator currents, which have been filtered to reduce the harmonic ripple for calculation. Currents i_a and i_b are summed to produce i_c as shown. The rotor speed is also input after getting converted to a DC voltage and scaled, like w_e to 1 volt = 200 radians per second. The w_r signal is inverted and multiplied by 10, however, for input to the multipliers. The current signals enter potentiometers which

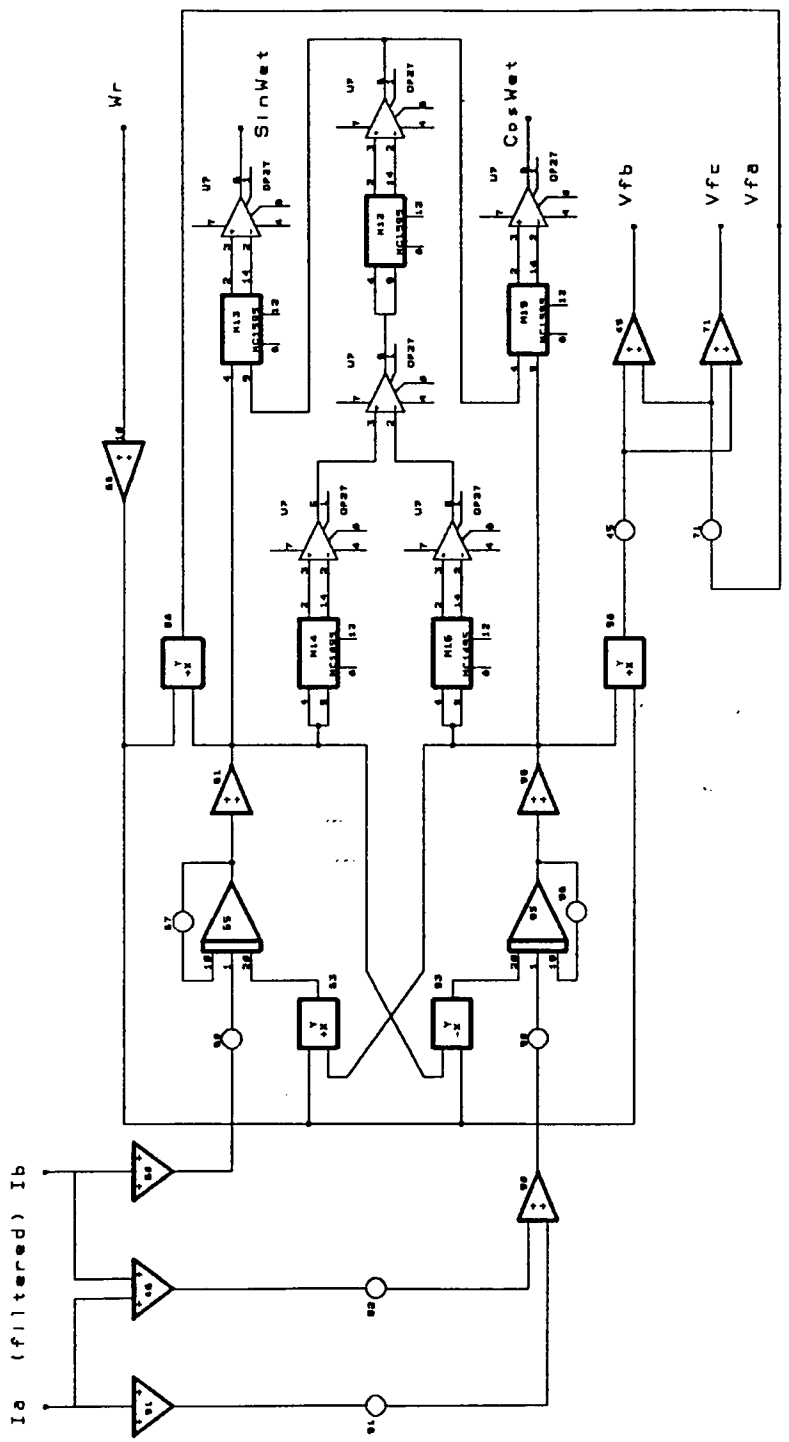


Figure 4-3: Flux, emf and unit vector calculation circuit

represent L_m/T_r. As mentioned in Chapter 3, L_m is the magnetizing inductance, and T_r is the effective rotor inductance to resistance ratio L_r/T_r. The values measured for this motor are:

$$L_m = 87 \text{ mH}$$

$$L_r = L = 8 \text{ mH}$$

$$R = 0.33 \text{ ohm}$$

$$L/R = 0.024$$

The figure shows how the scaling is set to produce the required outputs. In this case, the emf signals produced are 1/10 gain. For design simplicity of the division circuits, the unit vector currents are set at 4.5 V 0-peak, and then scaled to 1 volt 0-peak in the vector rotation circuit.

4.4 Hysteresis Band Calculation Circuit

This circuit takes its inputs from the vector rotation circuit, flux estimation circuit, and hand set variables (Figure 4-4). di^*/dt values are added with the V_f/L signals, scaled for 1 volt = 2000 A/sec and inverted on the computer. These signals are multiplied by L/kV_d (scaled 1 volt = 100,000 H/V) in multipliers 1, 2, and 3. The scaling for the succeeding multipliers is shown in the circuit diagram. Factored in multiplier M11 is $T_c = 1/f_c$ with a scale of 1 volt = 100 microseconds and $kV_d/4L$ scaled 1 volt = 10,000 V/H. The resulting scaling is set so that the values of the hysteresis bands are 1 volt = 1 amp for comparison with the actual and reference currents. The variable k is set with two potentiometers so that an extra multiplier would not be necessary. f_c^* is

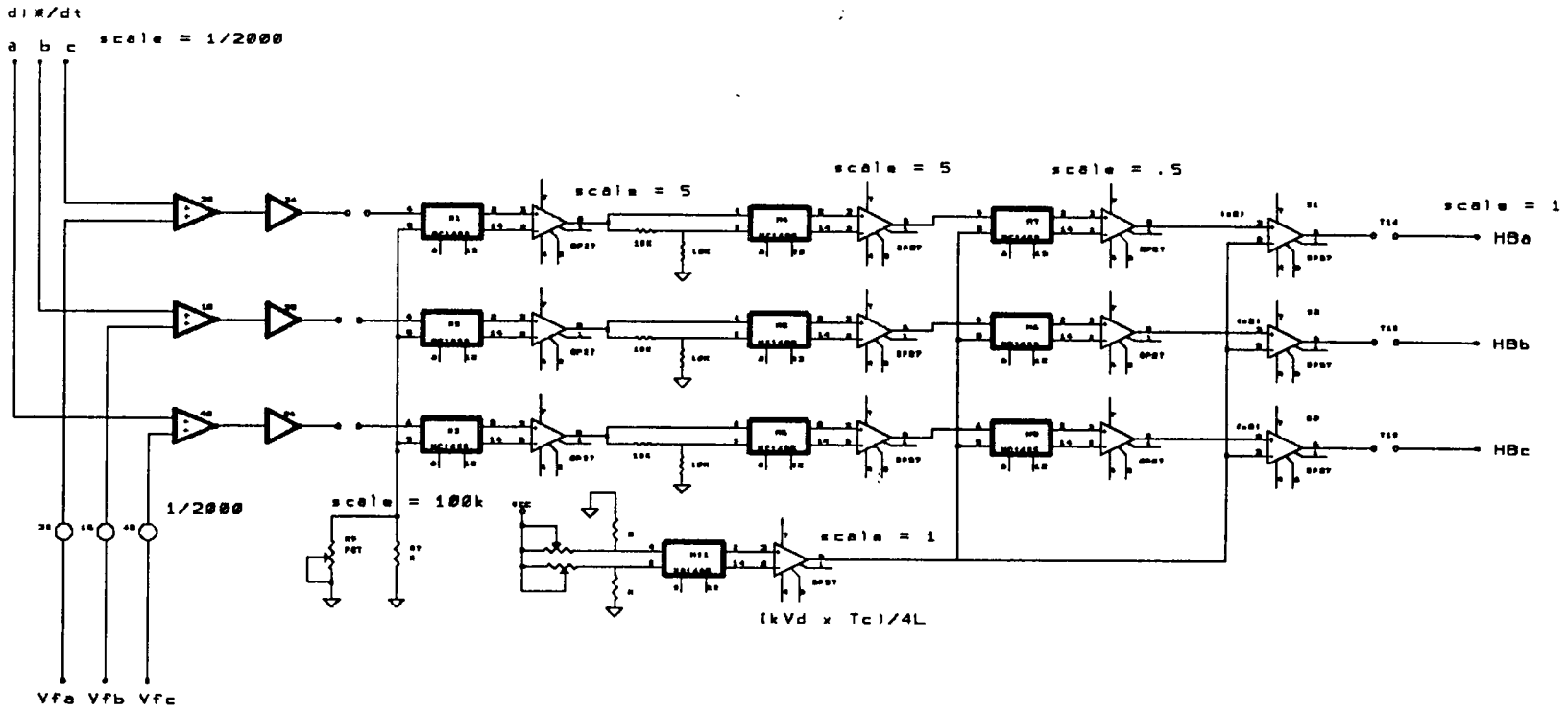


Figure 4-4: Hysteresis band calculation circuit

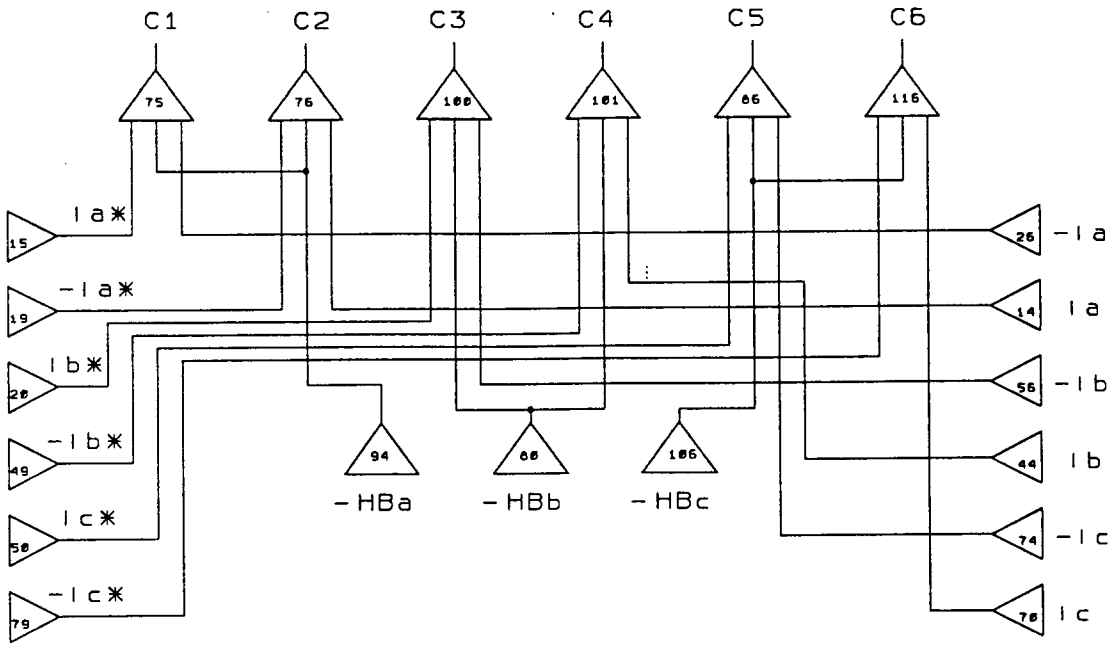
controlled in the circuit by the corresponding period value for simplicity also.

4.5 The Comparator Drive Circuit

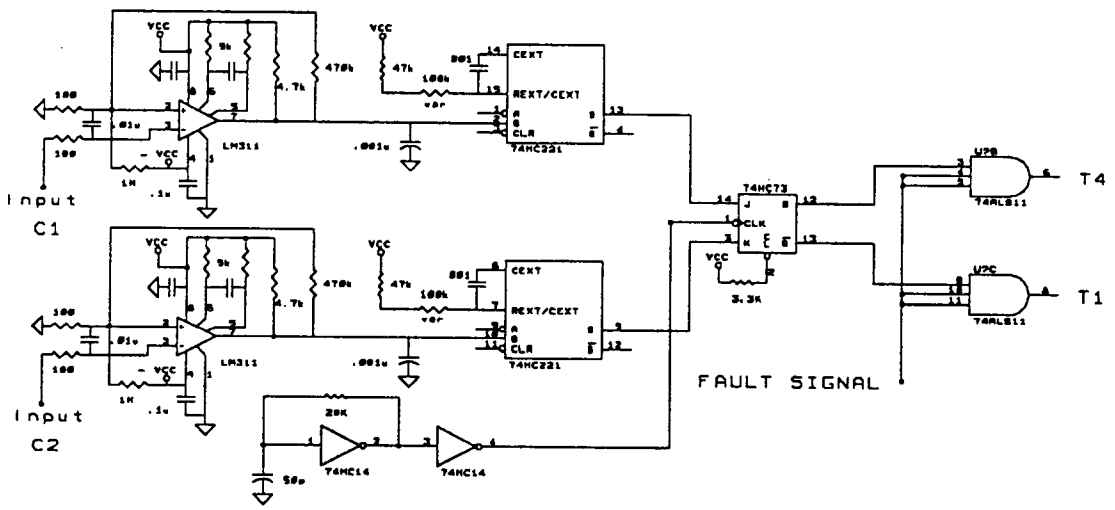
This circuit converts the analog computation signals to digital drive signals for the inverter. Figure 4-5a shows the combination of reference currents, unfiltered motor currents, and hysteresis band signals input to computer summers. The LM311 comparators have inverting outputs in this scheme, so they are fired with the appearance of a negative signal from the amplifiers. The amplifier inputs must be inverted as well so that the hysteresis band crossing points produce negative outputs. Figure 4-5b shows the comparator drive circuit for one phase. The feedback in the LM311 configuration is for preventing oscillations as mentioned in Chapter 3. A slow zero-crossing input from the amplifier, denoted by *C1* can cause high frequency oscillations with no feedback. Capacitors placed at the input and output of the comparator helped to solve this problem, while allowing frequencies ranging from about 100 Hz to 20 kHz to pass essentially undistorted. The one shot device is a 74HC221 monostable multivibrator with Schmitt Trigger inputs. A positive edge signal to the input creates a notch at the output with a predetermined pulse width

$$t_w = \ln 2 \; R_{ext} C_{ext} \tag{4.2}$$

The circuit uses the values C_{ext} = .001 uF and R_{ext} = 72 kOhm to produce a 50 usec pulse width. This is to prevent frequencies greater than 20 kHz from passing to the drive circuit. The flip-flop, as described in Chapter 3, is designed to latch the transistor drive



a: Comparator input



b: Circuit layout; one phase

Figure 4-5: Comparator and drive circuit

upon receiving a pulse from the one shot, and remain on until the opposite leg one shot fires a pulse. The flip-flop is clock driven by a simple RC feedback inverter circuit where R_c=20 kOhm, C_c=50 pF and f_{cl}= 1 MHz. It may be noted from the figure that the outputs to the transistors are reversed, or inverted. This is because the inverter module has opto-coupled drive inputs which gate the transistors with a zero input. The flip-flop outputs are AND gated, with the FAULT output signal from the inverter module to stop drive signals during fault conditions.

4.6 Feedback Signal Processing Circuits

The feedback signals used in the control system are the machine currents and rotor speed. Two phases of the currents are measured using current-to-voltage transformers which produce 0.1 volt/amp The unfiltered currents i_a,i_b are factored by 10 and summed to produce i_c and are all input to the comparator circuit. The flux synthesis circuit requires clean, synchronous frequency sinusoidal signals to generate usable emf and unit vector signals. Therefore, an active filter is required. A standard low-pass design used here is shown in Figure 4-6. The filter cutoff frequency is given by

$$f_p = \frac{1}{2\pi RC} = 400Hz \tag{4.3}$$

where $R=R1=R2=20$ kOhm and $C=C1=C2=0.02$ uF. Reducing the pass band further causes appreciable phase shift in the output, so a compromise must be made. Testing at 30 Hz showed fairly smooth waveforms and negligible phase shift. Also, testing of the flux circuit showed that the signals were further smoothed by the integrator circuits. The

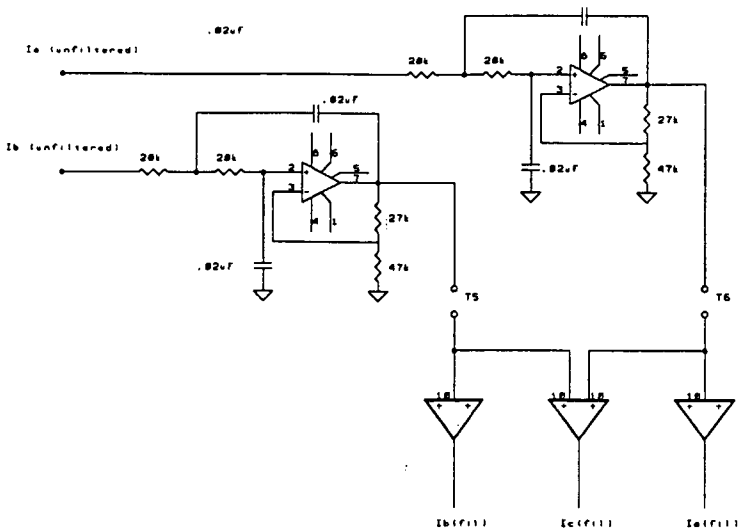


Figure 4-6: Current filter circuit

filtered currents are amplified by 10 for unity gain input to the flux circuit.

The rotor speed is measured using a Teledyne optical encoder mounted on the end of the rotor shaft. The encoder is a high-resolution device that produces 14,400 TTL pulses per revolution. The shaft speed for a 4-pole machine is half the rotor electrical speed, so a rotor frequency of 30 Hz corresponds to a pulse output of 216 kHz.

The frequency-to-voltage circuit operates effectively with an input range of about 50 kHz, therefore a divide-by-8 counter is used to reduce the encoder frequency as shown in Figure 4-7. The f-V converter operates such that the output voltage is described by

$$V_o = V_z f_i R_1 C_1 \tag{4.4}$$

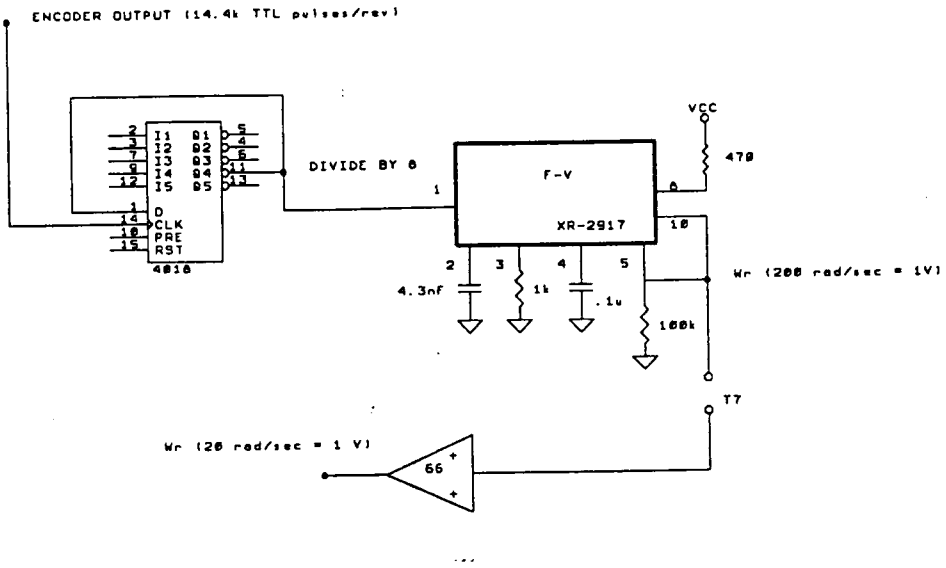


Figure 4-7: Frequency to voltage converter

where V_z, the IC zener voltage = 7.6 V, f_{in} is the input frequency, R_1 = 1200 Ohm and C_1 = 4.3 nF. This generates approximately 1 volt for a rotor speed of 30 Hz. Fine tuning for a scaling of 1 volt = 200 rad/sec is done with a computer potentiometer. The output is amplified with a gain of 10 for use in the emf circuit. A similar f-V circuit is built for measuring the switching frequency from one transistor drive signal.

4.7 Power Circuit

Figure 4-8 shows the inverter module and motor circuit. The module is an integrated rectifier and IGBT inverter with an isolated gate drive, rated for 500 V, 15 amp output. The module is supplied by a single phase 230 V line via a variable transformer to the diode rectifier. An 8 mF capacitor is connected across the DC link at the module

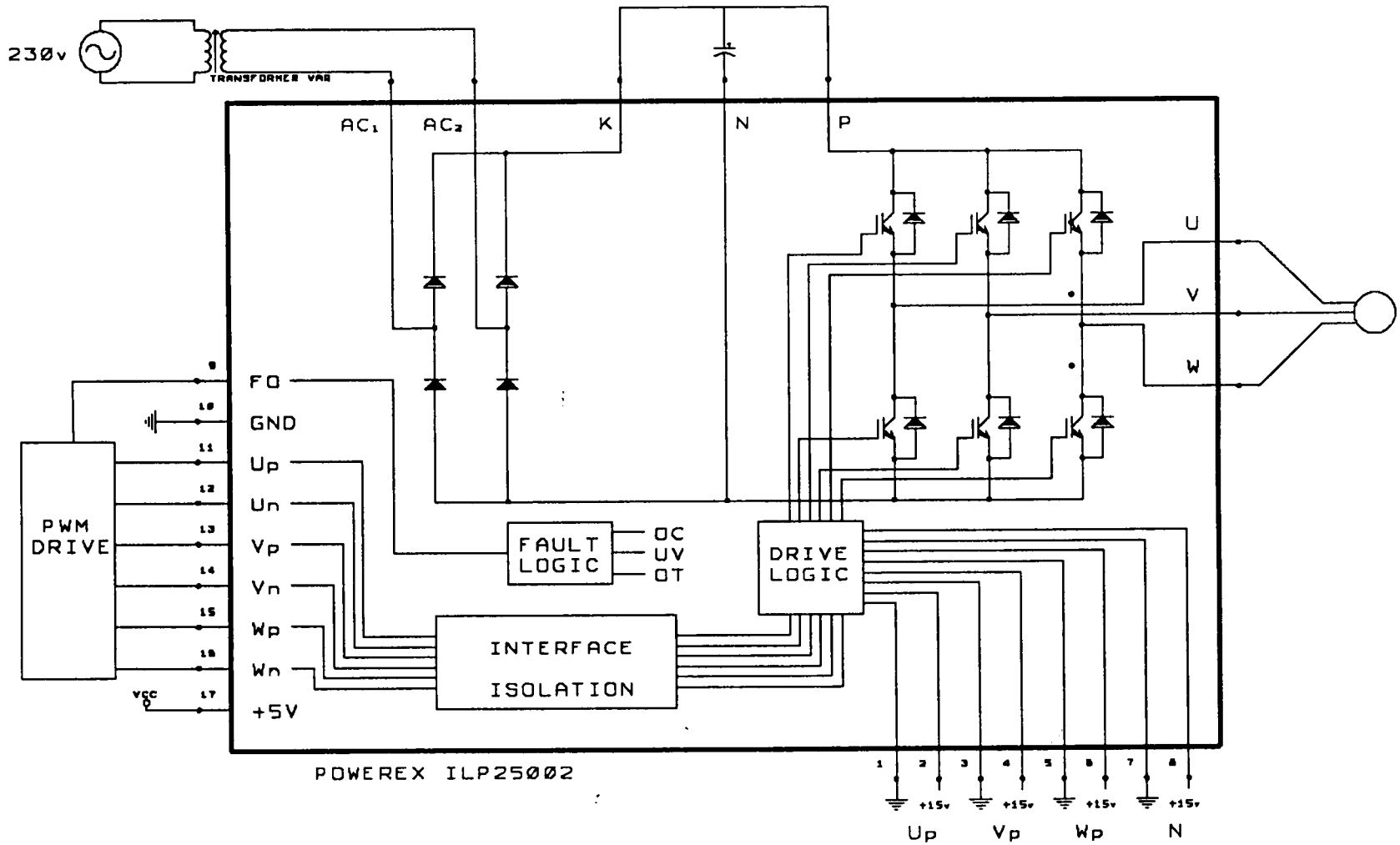


Figure 4-8: Power circuit and inverter module

terminals *K, P,* and *N* shown in the figure. Isolated supplies are required for terminals 1 through 8, one for each positive leg, and one for the combined negative legs as shown. Drive signals from the comparator circuit are sent to the isolated gate drive at terminals 11-16. The module incorporates its own lockout of 10 usec, and protection circuitry against overcurrent, undervoltage, and over-temperature. Any of these fault conditions sends a signal to *FO* which is input to the AND gates in the comparator circuit. Therefore, any fault condition will stop all drive signals to the module.

CHAPTER 5

SIMULATION STUDIES

An investigation of the proposed adaptive hysteresis band control is made in this chapter. Simulation studies using data from the 2 HP motor and test measurements are made of the bandwidth for no load and load conditions. Special attention is paid to the effect varying parameters has on the prescribed bandwidth and on overall operation. Finally some conclusions are made concerning the application of this type of control.

5.1 Switching Frequency Determination

Predictive analysis of the switching frequency in a hysteresis band controller is very difficult when using a machine with an unconnected neutral. The derivation of the hysteresis band in Chapter 2 illustrated the various voltage states that are applied across a phase of the machine, and the dependence these states have on the other two phase voltages. While the values of the voltage supplied to a phase during conduction of one transistor leg may vary between 2/3 V_d and 0, the variation is not completely random. A given switching state will have weighted tendencies in changing to its next state. Therefore, predicting switching state sequences would involve highly complex computations, and applying a random function of kV_d would indicate less order than actually exists. The point is illustrated by the zero switching state phenomenon that leads to a current error of $2HB$. Brod and Novotny [10] have described the case where a state in which devices *T1*, *T2*, and *T6* are conducting, therefore supplying a voltage of 2/3

V_d to phase *a*. If the current in phase *a* reaches the upper band limit before either of the other two phase states change, the next conducting state is *T4*, *T2*, and *T6*, which supplies a voltage of zero to phase *a*. If the emf in phase *a* is positive at this time, i_a will continue to rise even though the bottom transistor is conducting and may increase by as much as twice the hysteresis band value before another state change produces a reversal in direction. While this phenomenon is real, in practice it occurs rarely and does not affect overall rating considerations. It does, however, illustrate the complexities of predictive analysis. For that reason, a simple analysis of an expected average switching frequency is given here.

Application of the adaptive band is based on a selected switching frequency, so simulation of the band itself is entirely accurate. The average frequency is

$$\frac{\frac{di^+}{dt} + \frac{di^-}{dt}}{d} \tag{5.1}$$

where d is the distance (in amps) the current travels over a switching period. Since the emf is sinusoidal, the sum of $kV_d + V_f$ has no effect on the average voltage. Therefore

$$\frac{di}{dt}(ave) = \frac{\frac{1}{2}V_d}{L} \tag{5.2}$$

where 1/2 V_d is selected as the midpoint between 1/3 and 2/3. If the typical distance travelled in a switching cycle is $6HB$ (HB_c is constant) [10], then

$$f_{c(ave)} = \frac{\frac{1}{2}V_d}{6HB_cL} = \frac{V_d}{12HB_cL} \tag{5.3}$$

Selecting a frequency based on equation (5.3) provides a good starting point for implementation of the adaptive HB controller.

5.2 Hysteresis Band Simulation

Simulations of the hysteresis band were run using data from the motor and measured parameters during 30 Hz no-load operation. The hysteresis band formula is repeated for convenience (Equation 2.20):

$$HB = \frac{kV_d}{4f_c L}\left[1 - \frac{L^2}{k^2 V_d^2}\left(\frac{V_f}{L} + \frac{di^*}{dt}\right)^2\right] \tag{5.4}$$

The values given are:

$$V_d = 300 \text{ V}$$

$$L = 0.008 \text{ H}$$

The reference di^*/dt is calculated based on the reference current at no-load

$$i_{ref} = 5\sin\omega_e t$$

and

$$m = \omega_e \times 5\cos\omega_e t = 943\cos\omega_e t$$

(i^* is denoted by i_{ref} and di^*/dt is denoted by m in the simulations).

The emf at no-load was simulated at about 60 V 0-peak leading the reference current by 90 degrees. Therefore,

$$V_f = 50\cos\omega_e t$$

The frequency average calculated from Equation (5.3) is

$$\frac{V_d}{12\,HB_c\,L} = \frac{300}{12\,(.8)\,(.008)} = 4\ kHz$$

where the constant *HBc* is a conservative setting of 16% of the reference current. Figure 5-1 shows a two cycle simulation result of *HB* with an initial *k* of 2/3, and the band's relation to the reference current and emf. The graph shows an undesirably high band which peaks at over 1.5 amps. This gives a ripple current of over 30% of the reference. Notice also the relatively small modulation of the band as well, which may be effectively constant. This is because the modulating component of the band is inversely proportional to k^2. Therefore, when *k* is set high, the modulation is small. Figure 5-2 shows the same band with $k = 0.333$. The results here are much improved. The band modulates below the constant band setting of 0.8 amps. The peaks of the band correspond to the peaks of the reference current and zero crossings of the emf. This is desirable, as normally the average switching (upper and lower leg combined) is highest when the emf is low and the reference current is peaking (zero slope). The band maximum at this point allows switching speed to decrease. The average bandwidth is about 0.65 amps, which is slightly over 12% of the reference current. In higher power motor drives, the band may be a smaller fraction of the current.

In these low power motors, however, it is important to prevent the hysteresis band from becoming much less than one amp. Since switching frequency is related to the inverse of the band, a band modulating towards zero would not be helpful. In a microcomputer application, this can be avoided by using a SEARCH program that adjusts *k* based on the rotational frequency.

$k := 0.667$ $1/3 <= k <= 2/3$

$f := 4000$ desired sw frequency

$Vd := 300$ DC link voltage

$L := .008$ Motor leakage Inductance

$Vf_i := 60 \cdot \cos(\theta_i)$ EMF voltage

$m_i := 2 \cdot \pi \cdot 5 \cdot 30 \cdot \cos(\theta_i)$ reference di/dt

$iref_i := 5 \cdot \sin(\theta_i)$

$$HB_i := \frac{k \cdot Vd}{4 \cdot f \cdot L} \cdot \left[1 - \frac{L^2}{k^2 \cdot Vd^2} \cdot \left[\frac{Vf_i}{L} + m_i \right]^2 \right]$$

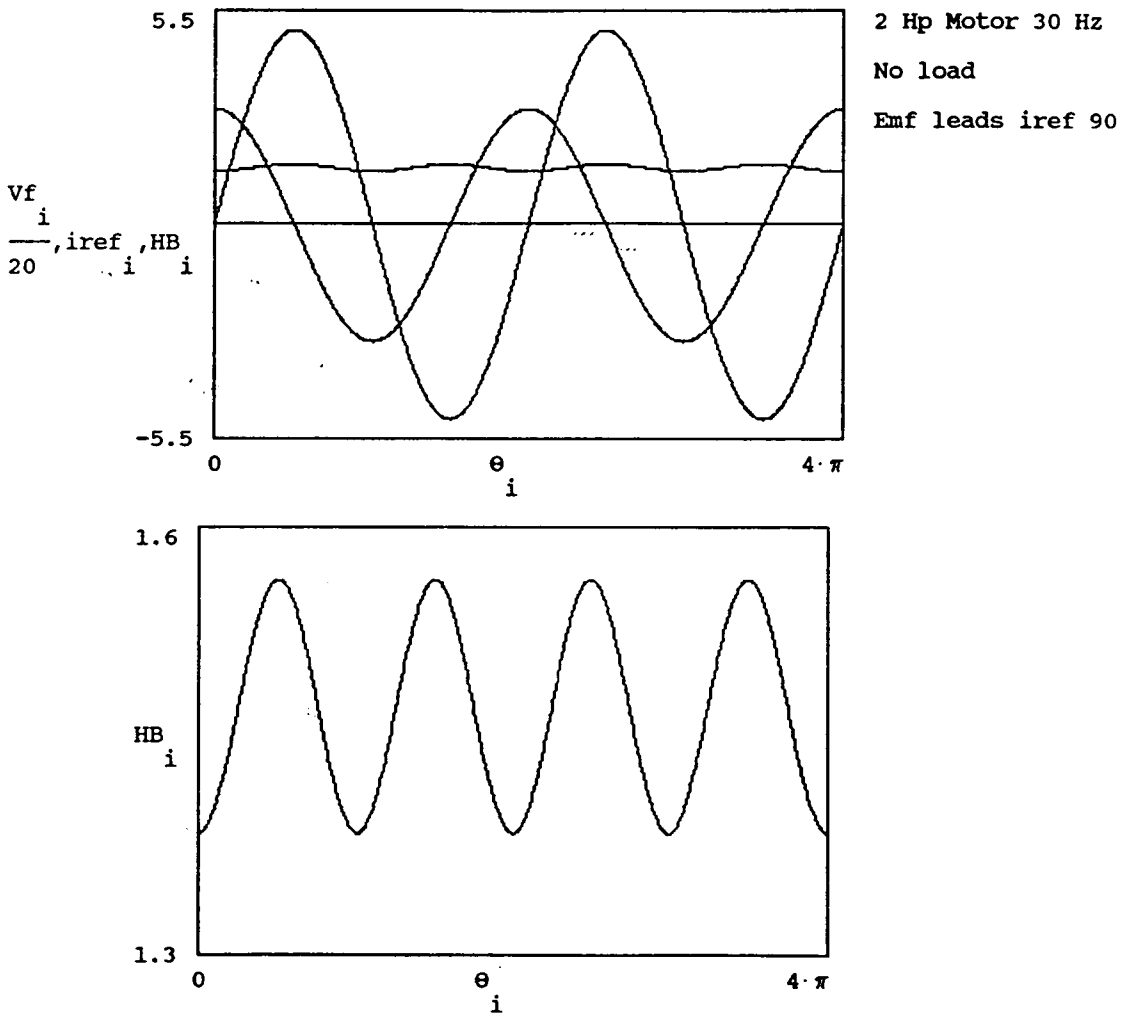


Figure 5-1: Hysteresis band simulation; no-load; k = 0.667

$k := 0.333$ $1/3 <= k <= 2/3$

$f := 4000$ desired sw frequency

$Vd := 300$ DC link voltage

$L := .008$ Motor leakage Inductance

$Vf_i := 60 \cdot \cos(\theta_i)$ EMF voltage

$m_i := 2 \cdot \pi \cdot 5 \cdot 30 \cdot \cos(\theta_i)$ reference di/dt

$iref_i := 5 \cdot \sin(\theta_i)$

$$HB_i := \frac{k \cdot Vd}{4 \cdot f \cdot L} \cdot \left[1 - \frac{L^2}{k^2 \cdot Vd^2} \cdot \left[\frac{Vf_i}{L} + m_i \right]^2 \right]$$

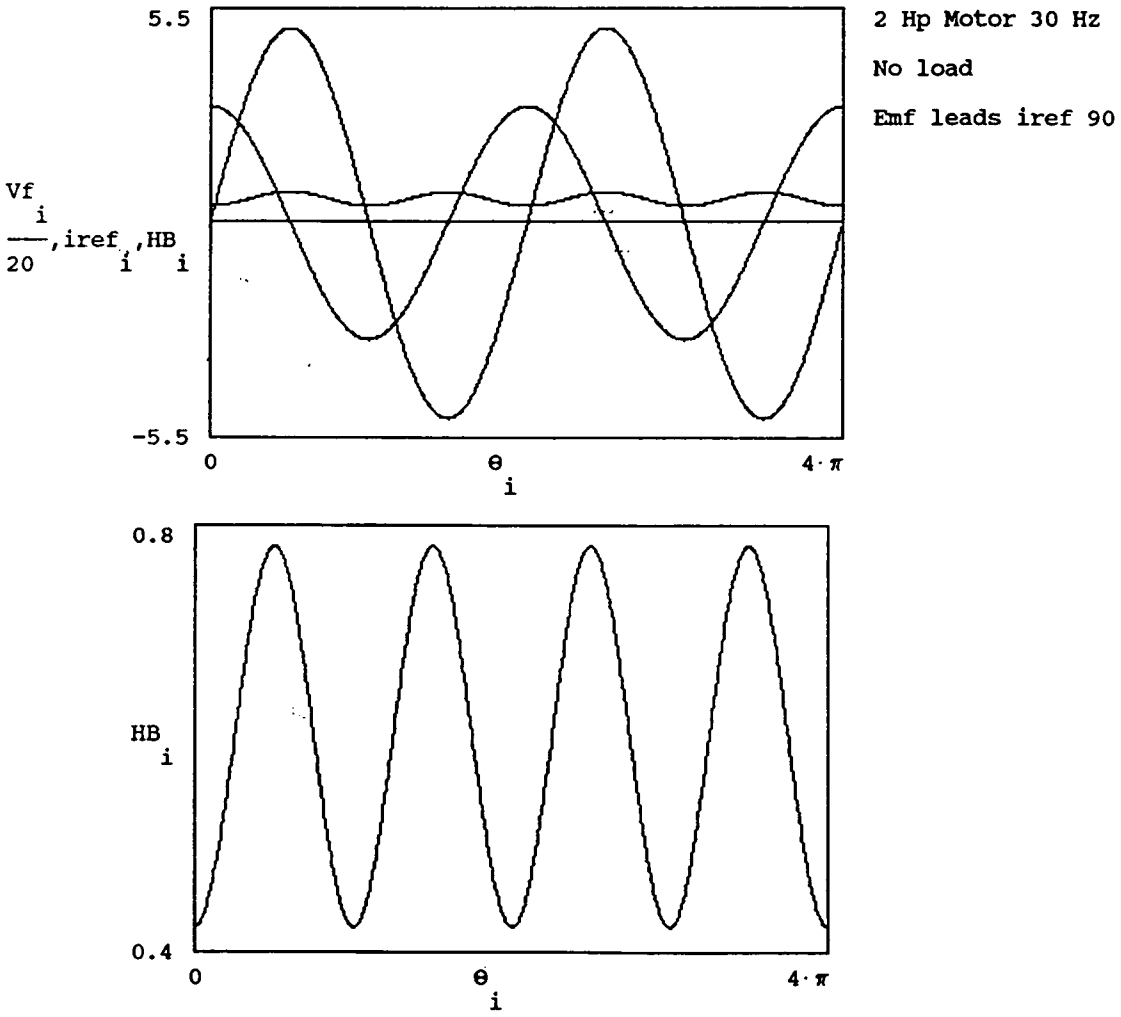


Figure 5-2: Hysteresis Band simulation; no-load; $k = 0.333$

K might therefore be set higher in low power drives than in high power ones.

Another test is made with simulation of a load. At near rated torque and reduced flux, the emf drops some in magnitude and leads the reference current wave by about 45 degrees. Figure 5-3 shows the resulting band and its relation to the reference current and emf. Note again the coinciding of the band peaks with the emf zero crossings. This again is desirable, and helps to prevent output current phase lag and DC offsets which occur during constant band operation. It should also be emphasized that the results in this test show optimum bandwidth characteristics for a given desired frequency, but not necessarily optimum overall performance. Setting an optimum *k* and average frequency is dependent on monitoring of the actual switching frequency, which is not simulated here.

5.3 Bandwidth Sensitivity to Leakage Inductance Variation

While it is evident from Equation (5.4) that the hysteresis band is significantly affected by variation of the leakage inductance, simulations are shown here to illustrate the point. As mentioned before, it has been shown that the effective leakage inductance of an inverter driven induction motor decreases with increased motor speed. [7] Variations in the inductance are inversely proportional to the machine current slopes, and therefore the switching frequency. Updating *L* with a lookup table for the motor frequency range would be helpful in creating an optimum band. However, in doing so, constant updating of *k* and the selected frequency would be required.

$k := 0.333$ $1/3 <= k <= 2/3$

$f := 4000$ desired sw frequency

$Vd := 300$ DC link voltage

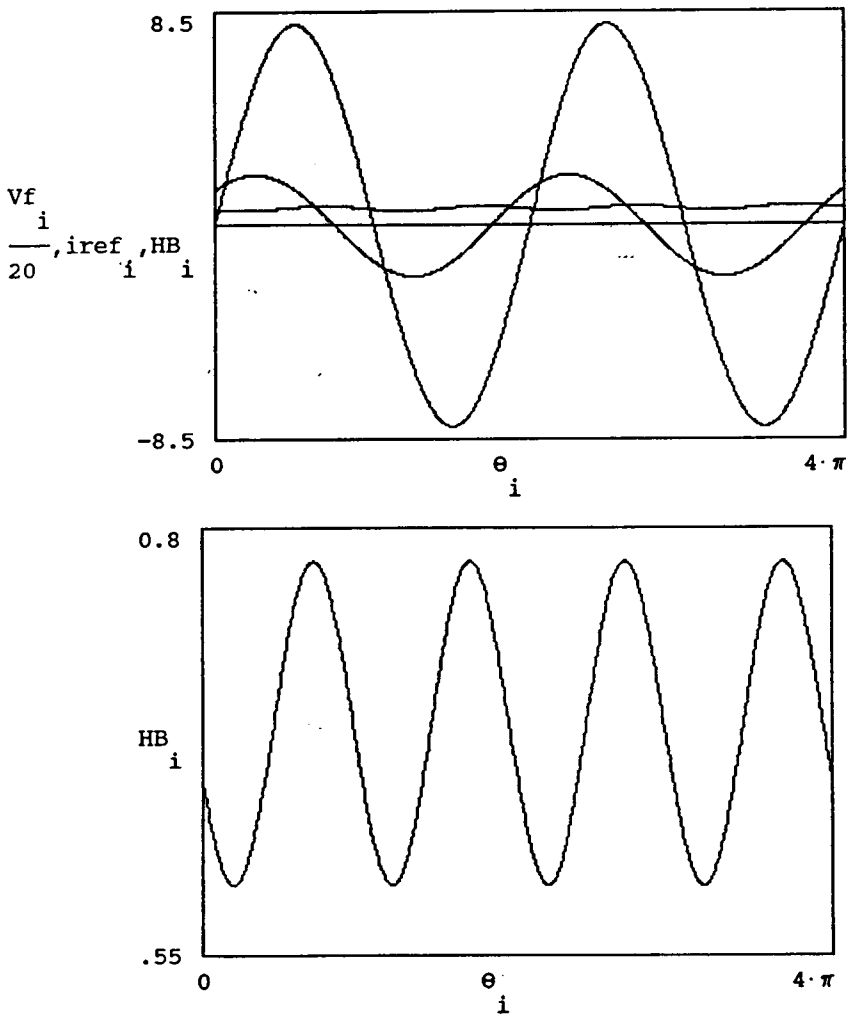
$L := .008$ Motor leakage Inductance

$$Vf_i := 40 \cdot \cos\left[\theta_i - \frac{\pi}{4}\right]$$ EMF voltage

$$m_i := 2 \cdot \pi \cdot 8 \cdot 30 \cdot \cos[\theta_i]$$ reference di/dt

$$iref_i := 8 \cdot \sin[\theta_i]$$

$$HB_i := \frac{k \cdot Vd}{4 \cdot f \cdot L} \cdot \left[1 - \frac{L^2}{k^2 \cdot Vd^2} \cdot \left[\frac{Vf_i}{L} + m_i\right]^2\right]$$



2 Hp Motor 30 Hz

Load

Emf leads iref 45

Figure 5-3: Band simulation with torque loading

Figures 5-4 and 5-5 show resulting bandwidths for decreased and increased leakage inductance, respectively. The changes are exaggerated to show the sensitivity of the bandwidth to its variation. It is clear that updating L, which would be a result of updated w_r and di/dt would require updating of k and $f_{c(ave)}$ as well.

$k := 0.333$ $1/3 <= k <= 2/3$

$f := 4000$ desired sw frequency

$Vd := 300$ DC link voltage

$L := .003$ Motor leakage Inductance

$Vf_i := 70 \cdot \cos(\theta_i)$ EMF voltage

$m_i := 2 \cdot \pi \cdot 5 \cdot 40 \cdot \cos(\theta_i)$ reference di/dt

$iref_i := 5 \cdot \sin(\theta_i)$

$$HB_i := \frac{k \cdot Vd}{4 \cdot f \cdot L} \cdot \left[1 - \frac{L^2}{k^2 \cdot Vd^2} \cdot \left[\frac{Vf_i}{L} + m_i \right]^2 \right]$$

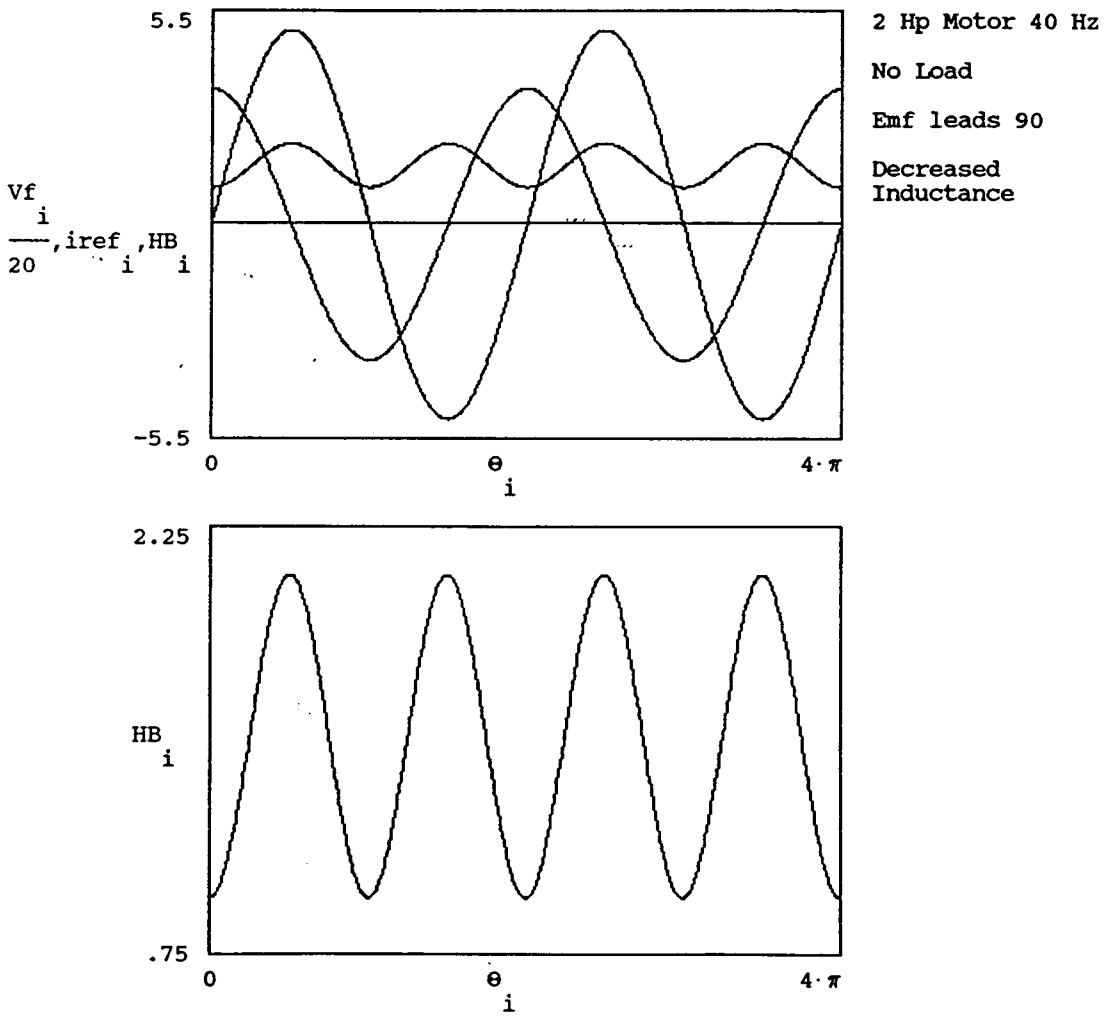


Figure 5-4: Hysteresis band with decreased leakage inductance

$k := 0.333$ $1/3 <= k <= 2/3$

$f := 4000$ desired sw frequency

$Vd := 300$ DC link voltage

$L := .013$ Motor leakage Inductance

$Vf_i := 50 \cdot \cos(\theta_i)$ EMF voltage

$m_i := 2 \cdot \pi \cdot 5 \cdot 20 \cdot \cos(\theta_i)$ reference di/dt

$iref_i := 5 \cdot \sin(\theta_i)$

$$HB_i := \frac{k \cdot Vd}{4 \cdot f \cdot L} \cdot \left[1 - \frac{2 \cdot L^2}{k^2 \cdot Vd^2} \cdot \left[\frac{Vf_i}{L} + m_i \right]^2 \right]$$

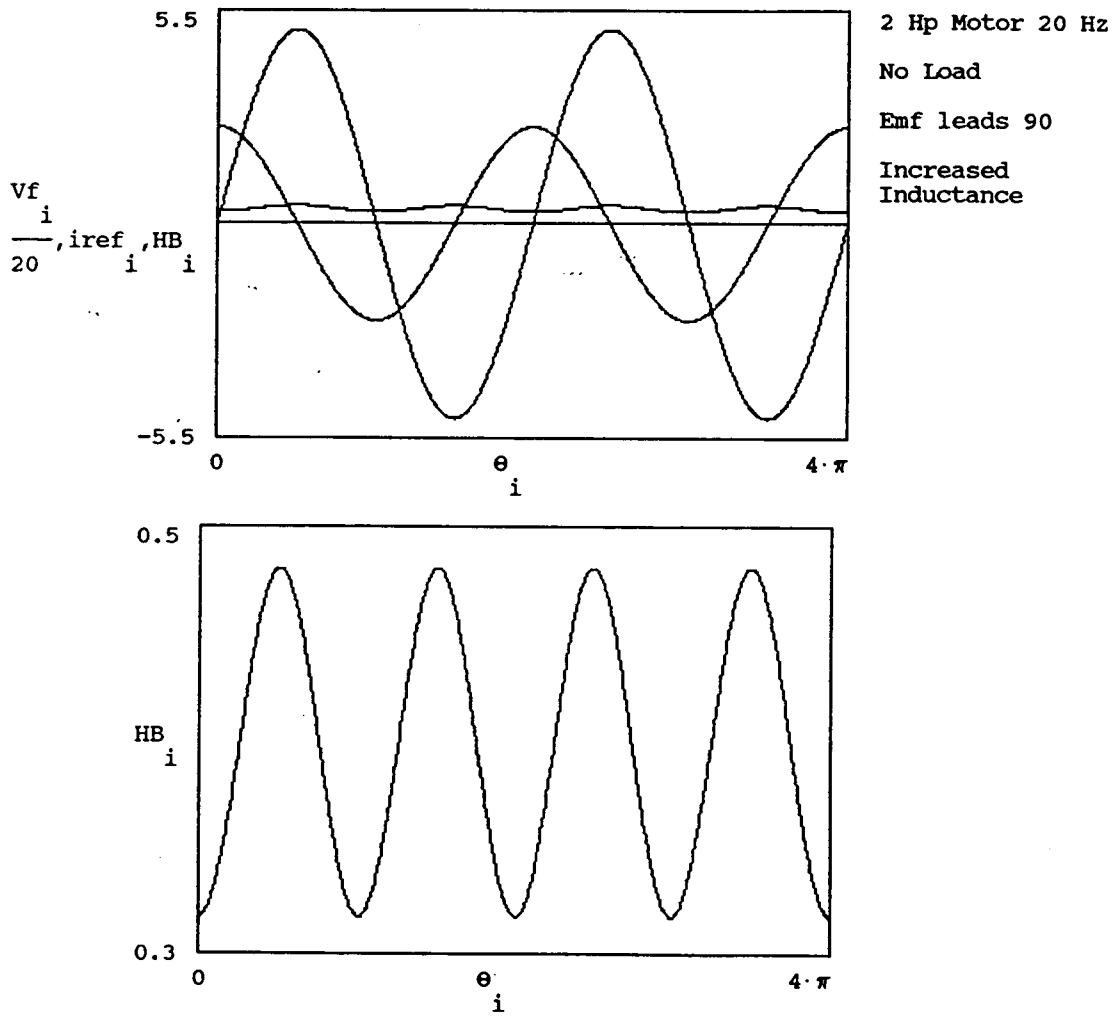


Figure 5-5: Hysteresis band with increased leakage inductance

CHAPTER 6

LABORATORY TEST RESULTS

This chapter presents results obtained from laboratory tests of the prototype hysteresis band control system. Tests on each hardware subsystem are performed using simulated system operating conditions. All tests are made for no load operation of the motor at 30 Hz. Results are given for each of the relevant computer and hardware generated waveforms.

6.1 Flux, Emf and Unit Vector Calculation

Two simulated current waveforms representing machine currents i_a and i_b are generated to test the flux, emf and unit vector circuit. Based on motor tests for no load and 30 Hz operation, the currents are valued at 5 amps 0-peak, with 1 volt to 1 amp scaling. Fluxes are calculated using the method described in Section 3.2, based on knowledge of the magnetizing inductance, rotor leakage inductance and resistance , with measured values of w_r and machine currents. The integrator circuit produced stationary *d-q* axis flux components, with 90 degree displacement. Figure 6-1 shows the flux signals measured from computer amplifiers 61 and 96 with voltage values of approximately 6.5 volts 0-peak. In the figure, the leading flux is the *d* axis component and the lagging flux is the *q* axis component. Scaling for the flux components are 1 volt = .05 weber, so the flux values are approximately 0.325 weber 0-peak. The signals are then calculated by multiplying the flux signals by w_r. Scaling for w_r is 1 volt = 20

2 V/div

1 ms/div

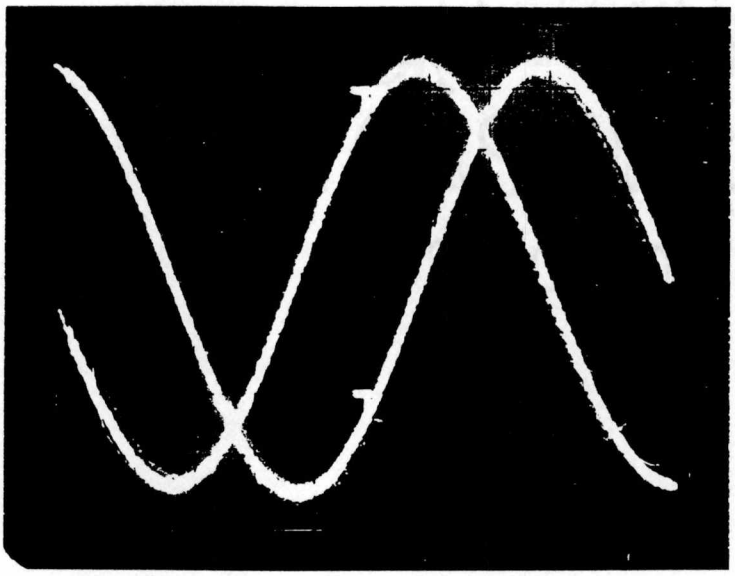


Figure 6-1: *d-q* axis flux signals

rad/sec in this circuit, so for 30 Hz operation with a very small slip, w_r is set to 0.92 volts. This gives an emf representation of approximately 6 volts. The phase *a* and *b* emf waveforms shown in Figure 6-2 are scaled 1 volt = 10 (actual) volts, so the emf values calculated for no load are approximately 60 volts. The emf signals have also been correctly converted to 3-phase, as V_{fa} leads V_{fb} by 120 degrees. To test the emf wave for accurate representation of a no load condition, the emf in phase a is compared with i_a^* in Figure 6-3. Ideally, no load current lags the emf by 90 degrees, but friction and the encoder shaft mount will inject a small shift. In the figure, the emf is the higher peaked signal and leads the current by just under 90 degrees.

The unit vector signals are simply created from the normalized flux signals in Figure 6-1, and scaled to 1 volt 0-peak. $Sinw_e t$ is represented by the *q* axis flux and

2 V/div

2 ms/div

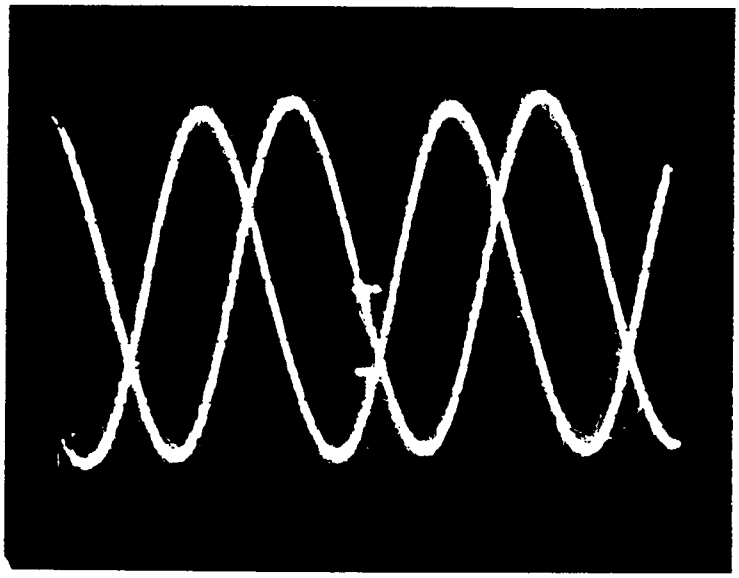


Figure 6-2: Phase *a* and *b* emf signals

V_{fa}: 2 V/div

i_a^*: 5 V/div

2 ms/div

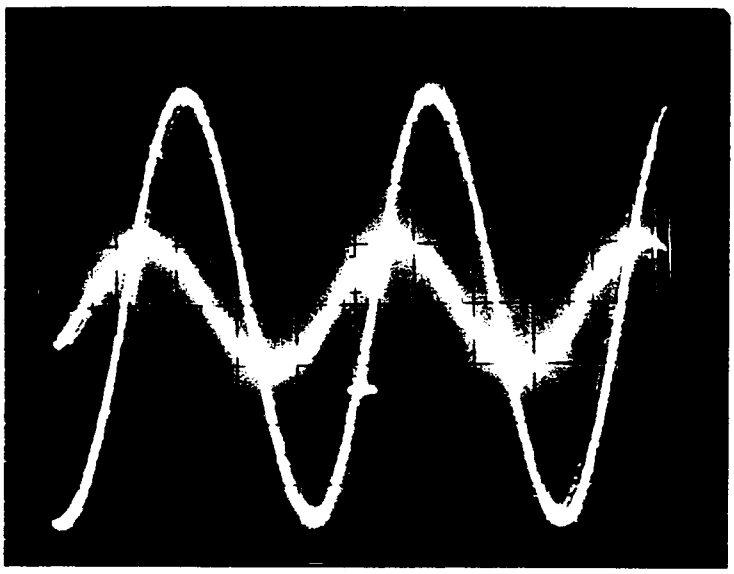


Figure 6-3: Phase *a* emf and di^*/dt signals

$cosw_e t$ is represented by the *d* axis component. These results show that the analog computer's computational capabilities in real time are excellent.

6.2 Vector Rotation and Current Differentiation Circuit

This circuit uses the unit vector signals to generate and differentiate the 3-phase reference currents i_a^*, i_b^*, and i_c^*. Generating the reference currents is done simply by transforming the synchronously rotating currents i_{qe}^* and i_{de}^* to stationary components i_{qs}^* and i_{ds}^*, and then from 2-phase to 3-phase signals. Figure 6-4 shows currents i_a^* and i_b^* to be 5 volts 0-peak representing 1 amp per volt, and displaced by 120 degrees. Differentiation of the currents is performed by multiplying w_e by the stationary *d-q* axis

2 V/div

1 ms/div

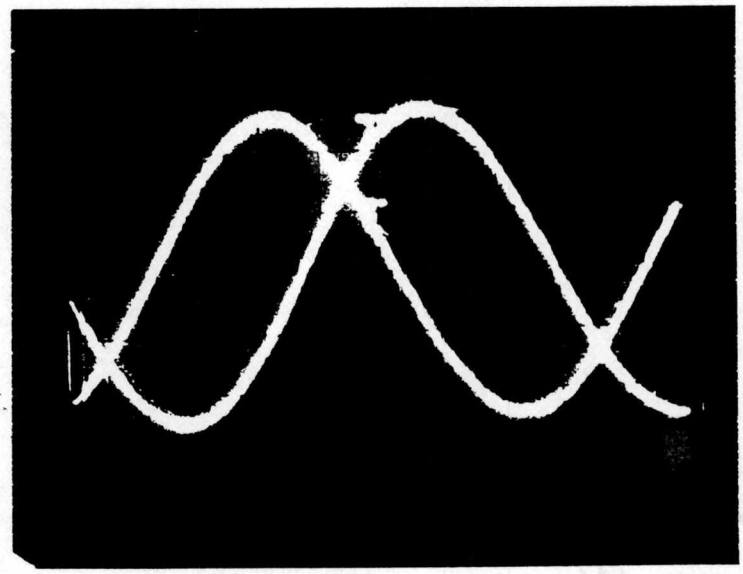


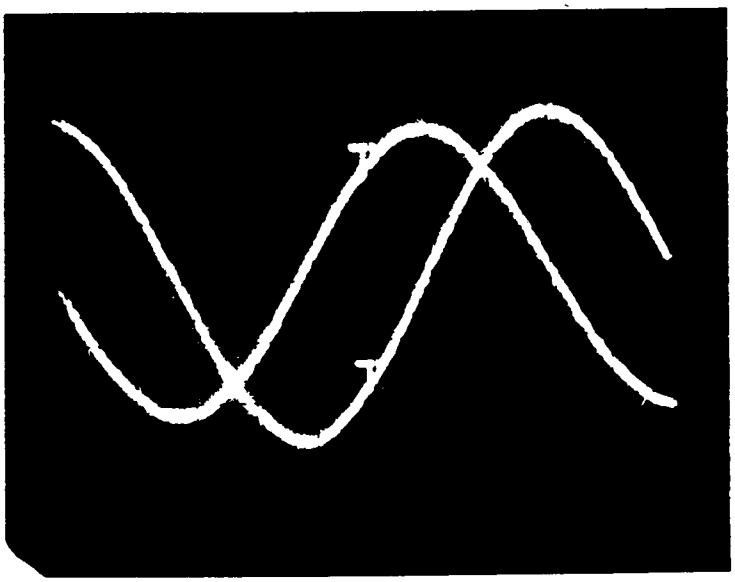
Figure 6-4: Phase *a* and *b* reference currents

components and algebraically defining the derivatives as described in Section 3.3. Figure 6-5 shows the differentiated current di_a^*/dt, with respect to i_a^*. In the figure,

$$i_a^* = 5\sin\omega_e t$$

so,

$$\frac{di_a^*}{dt} = \frac{5}{200} \times \frac{377}{2} \cos\omega_e t = 4.71\cos\omega_e t$$



2 V/div

1 ms/div

Figure 6-5: Phase a reference and differentiated current

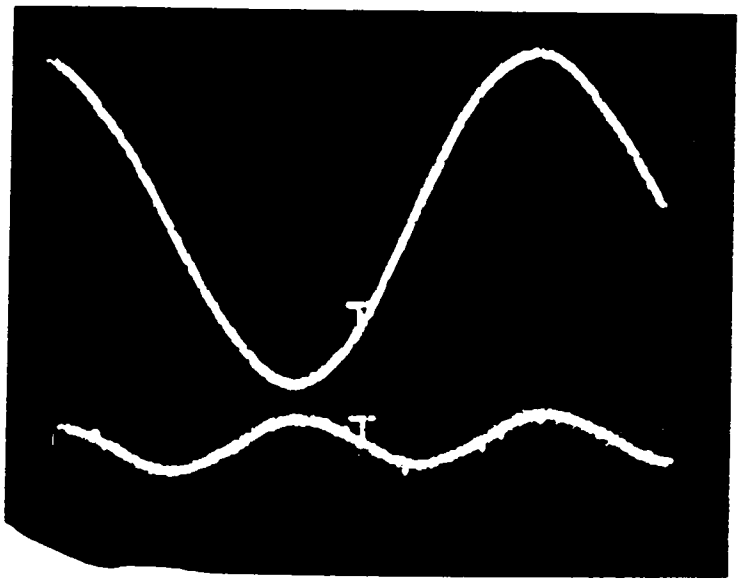
6.3 Hysteresis Band Calculation

The hysteresis band calculation circuit gave excellent results. Calculations based on the scaled parameters and generated signals described in Section 3.4 produced *HB* waveforms nearly identical to those simulated in Chapter 5. Figures 6-6a and 6-6b show

i_a^*: 2 V/div

HB: .5 V/div

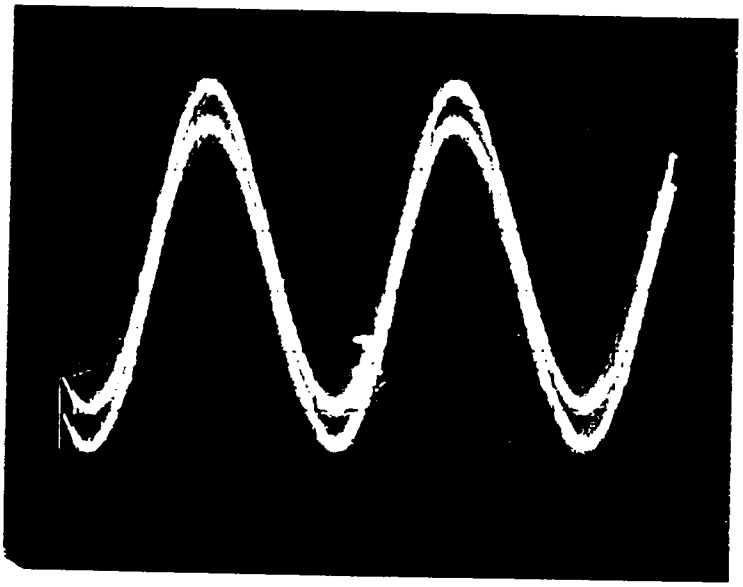
1 ms/div



a: Band with reference

2 V/div

2 ms/div



b: Summed signals with reference

Figure 6-6: Phase *a* hysteresis band and reference current

the hysteresis band in phase *a* with the reference current. In Figure 6-6a, the band is modulating between approximately 0.5 and 0.8 amps, and is in the correct phase relation to the reference current for no load conditions. Figure 6-6b shows the sum of the two signals compared with i_a^*. The reference current is the bottom signal and is symmetrical to the *x* axis. The summed signal shows the maximum band at the reference peaks, and the minimum band at the reference zero crossing. The computation used the average switching frequency of 4 kHz calculated in Chapter 5, and a value of *k* near 0.333.

6.4 Comparator and Drive Circuit

Tests of the comparator and drive circuit were conducted for a switching frequency range of 100 Hz to 20 kHz to ensure safe operation free from oscillatory effects. The tests showed only slight, insignificant shift due to the comparator input capacitors at 20 kHz. Simulation results of 4 kHz operation are given here. Figure 6-7a shows three of the comparator circuit waveforms. The top waveform is the input to the LM311 comparator driving T_1. The input is governed by the sum

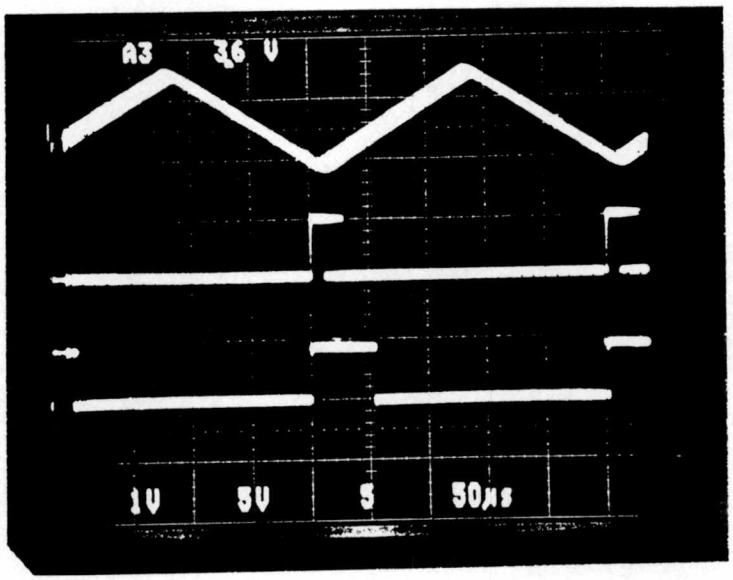
$$i_a - (i_a^* - HB_a)$$

which produces a negative zero crossing when the actual current is below the reference minus *HB*. The actual current is simulated by summing the reference current with a 1 volt 4 kHz triangle wave. The resulting sum of the three signals is a 4 kHz triangle wave with bottom peaks just below zero. The second waveform is the comparator inverted output, which is on only as long as the triangle wave is less than zero. The bottom signal is the subsequent one-shot output. The one shot sets a minimum pulse width of

Comp In:
1 V/div

5 V/div

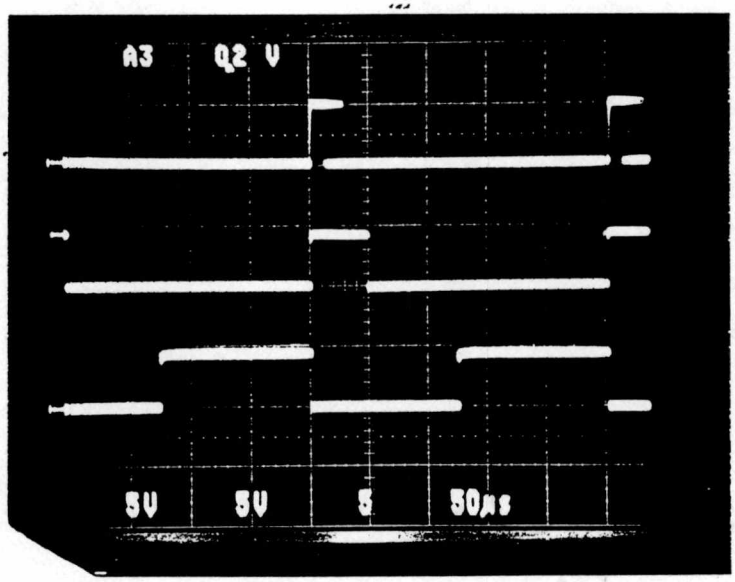
50 us/div



a: Comparator input and output; one shot

5 V/div

50 us/div



b: With flip flop output

Figure 6-7: Comparator and drive circuit waveforms

50 microseconds (20 kHz) for the drive as shown. Figure 6-7b shows the comparator and one-shot output with the output of the flip flop (bottom). The inverter module drive fires the transistor upon receiving a low input signal, so the flip flop output is inverted. Transistor drive signals for one leg are simply the inverting and non-inverting flip flop outputs. Protection from shoot-through fault current is provided in the inverter module, which has a built-in 10 microsecond lock-out. The comparator drive circuit provided excellent response in the frequency operating zone as shown.

Because of defective transistor legs in the inverter modules tested, the motor drive could only be simulated in the end. Figure 6-8 shows the simulated machine phase current i_a at 30 Hz and no load conditions, and with a constant switching frequency of 4 kHz. Although the switching states are not simulated here, the working results of the completed subsystems suggest that the simulation is sufficiently accurate.

2 V/div

2 ms/div

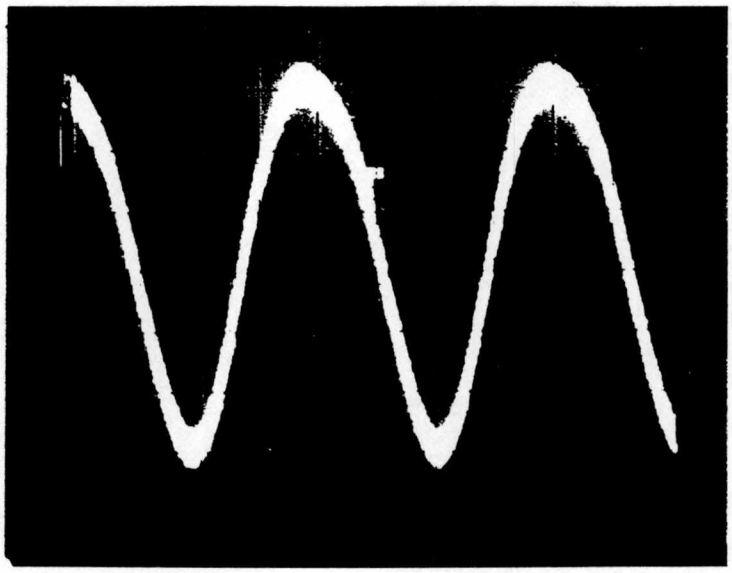


Figure 6-8: Simulated motor phase current

CHAPTER 7

CONCLUSION

An investigation of an adaptive hysteresis band PWM induction motor controller demonstrates its potential for high performance machine drives. While the standard hysteresis band control method is uncomplicated in implementation, the adaptive method presented here can be readily applied in existing vector control drives, where the required parameters are already utilized.

The advantages of such a scheme are numerous. This paper has shown through computer simulation and laboratory tests that a modulating hysteresis band control technique applied to an induction motor drive can reduce the switching frequency variations problem that constant-band methods exhibit. A more constant inverter frequency reduces harmonic heating and losses in the machine. Phase lag and offset between command and actual currents, resulting from the motor's counter emf, can also be controlled. The incorporation of an independent control variable allows for versatility in optimization criteria. A study of the control technique was also presented that analyzes motor parameter variation and power considerations. The method's adaptation to induction motor characteristics was demonstrated with the design, construction and testing of a prototype system.

As power semiconductor devices continue to improve in rating and speeds, variable AC drive systems, such as the prototype developed here, will become the standard in high power, high performance applications.

REFERENCES

References

[1] Murphy, J.M.D. and F.G. Turnbull, Power Electronic Control of AC Motors, New York, Pergamon Press, 1988.

[2] Bose, B.K., "Adjustable Speed AC Drives - A Technology Status Review," Proceedings of the IEEE, Vol. 70, No. 2, February, 1982.

[3] Bose, B.K., "Power Electronics - An Emerging Technology," IEEE Transactions on Industrial Electronics, Vol. 36, No. 3, August, 1989.

[4] Bose, B.K., "An Adaptive Hysteresis-Band Current Control Technique of a Voltage Fed PWM Inverter for Machine Drive System," Proceedings of the IEEE, October, 1988.

[5] Bose, B.K., Power Electronics and AC Drives, Englewood Cliffs, N.J., 1986.

[6] Plunkett, A.B., "A Current Control PWM Transistor Inverter Drive," Conf. Rec. IEEE/IAS 1979 Annual Meeting, 1979.

[7] Honsinger, V.B., "Induction Motors Operating From Inverters," Conf. Rec., IEEE/IAS Annual Meeting, October, 1980.

[8] EAI, Parallel Analog Processor Reference Handbook, W. Long Branch, N.J., Electronic Associates, May 1975.

[9] Motorola, Specifications and Applications Information, Phoenix, AZ, 1988

[10] Brod, D.M., and D.W. Novotny, "Current Control of VSI-PWM Inverters," IEEE Transactions on Industrial Applications, Vol IA-21, 1985.

[11] Fitzgerald, A.E., and C. Kingsley, Electrical Machinery, New York, McGraw-Hill, 1952.

VITA

Gregory James Ball was born in Oak Ridge, Tennessee on May 30, 1964. Upon graduating from Oak Ridge High School in 1982, he enrolled in the College of Engineering at Tulane University in New Orleans. He was accepted for participation in Tulane's Junior Year Abroad honors program and attended the University of Newcastle-Upon-Tyne in England during the 1984-1985 school year. He then returned to New Orleans and in May of 1986 received a Bachelor of Science degree in Electrical Engineering.

Through a work exchange program sponsored by the American Scandinavian Foundation, he spent the following year at the Department of Power Electronics and Electrical Machines at Chalmers University in Gothenburg, Sweden. There he helped with the development of the department's wind power system located on an island nearby.

In the fall of 1987 he accepted a research assistantship at the University of Tennessee, Knoxville and began study toward a Master's degree specializing in power electronics. Upon graduation, he plans to continue working with power generation from wind and other renewable energy sources.